# The mechanism of full activation of tumor suppressor PTEN at the phosphatidylinositol-enriched membrane

Hyunbum Jang[1,*], Iris Nira Smith[2,*], Charis Eng[2-5,†], Ruth Nussinov[1,6,†]

[1]Computational Structural Biology Section, Frederick National Laboratory for Cancer Research in the Laboratory of Cancer Immunometabolism, National Cancer Institute, Frederick, MD 21702, U.S.A.

[2]Genomic Medicine Institute, Cleveland Clinic Lerner Research Institute, Cleveland, OH 44195, U.S.A.

[3]Center for Personalized Genetic Healthcare, Cleveland Clinic Community Care and Population Health, Cleveland, OH 44195, U.S.A.

[4]Department of Genetics and Genome Sciences, Case Western Reserve University School of Medicine, Cleveland, OH 44106, U.S.A.

[5]Germline High Risk Cancer Focus Group, Comprehensive Cancer Center, Case Western Reserve University School of Medicine, Cleveland, OH 44106, U.S.A.

[6]Department of Human Molecular Genetics and Biochemistry, Sackler School of Medicine, Tel Aviv University, Tel Aviv 69978, Israel

*These authors contributed equally and are considered joint first authors

[†]Corresponding authors

Correspondence should be addressed to:

Ruth Nussinov

Frederick National Laboratory for Cancer Research

Frederick, MD 21702, U.S.A.

Phone: 301-846-5579

E-mails: NussinoR@mail.nih.gov

## Abstract

Tumor suppressor PTEN dephosphorylates signaling lipid $PIP_3$ produced by PI3Ks. Abundant $PIP_3$ promotes cell growth and proliferation. PTEN is the second most highly mutated protein in cancer and is drugless. The detailed mechanism at the membrane of this pivotal phosphatase is unknown hindering understanding and drug discovery. Here for the first time, exploiting explicit solvent simulations, we tracked full-length PTEN trafficking from the cytosol to the membrane, its interaction with membranes composed of zwitterionic phosphatidylcholine and anionic phosphatidylserine and phosphatidylinositol, including signaling lipids $PIP_2$ and $PIP_3$, and moving away from the zwitterionic and getting absorbed onto the anionic membrane that harbors the $PIP_3$. $PIP_3$ then allosterically unfolds the N-terminal $PIP_2$ binding domain, translocating it to the membrane where its polybasic motif interacts with $PIP_2$, localizing on microdomains enriched in signaling lipids, as PI3K does. Finally, we determined PTEN catalytic action at the membrane, all in line with available experimental observations.

**Keywords:** phosphatase, dephosphorylation, signaling lipid, phosphatidylinositol, $PIP_3$, $PIP_2$, protein-membrane interaction, Ras

## Introduction

Tumor suppressor phosphatase and tensin homolog (PTEN) dephosphorylates phosphatidylinositol 3,4,5-trisphosphate ($PIP_3$) to phosphatidylinositol 4,5-bisphosphate ($PIP_2$) (Chalhoub and Baker, 2009). Signaling lipid $PIP_3$, a major product of phosphatidylinositol 3-kinases (PI3Ks), recruits a subset of proteins, phosphoinositide-dependent protein kinase 1 (PDK1) and AKT to the plasma membrane, leading to cell growth, survival, and migration (Fruman et al., 2017). Both PTEN and PI3K are among the most frequently mutated proteins in malignancies, acting as negative and positive regulators in the PI3K/AKT/mTOR pathway (Chalhoub and Baker, 2009; Song et al., 2012). Countering PI3K lipid kinase activity, PTEN lipid phosphatase suppresses the level of $PIP_3$ in the cell membrane. In many cancers, elevation of $PIP_3$ levels are linked to increased activity of PI3K in the oncogenic state (Fruman et al., 2017). In human malignancies, both sporadic (Yehia et al., 2019) and heritable (Yehia et al., 2018) loss of PTEN function by respectively, somatic and germline mutations, deletions, posttranslational modifications, and phosphorylation leads to $PIP_3$ accumulation in the cell membrane, boosting unrestrained PI3K-stimulated cell proliferation (Alvarez-Garcia et al., 2019; Dillon and Miller, 2014; Kotelevets et al., 2020; Song et al., 2012).

With 403 amino acids, PTEN is composed of the N-terminal $PIP_2$ binding domain (PBD aka PBM, $PIP_2$ binding motif, residues 1-15), the phosphatase domain (residues 16-185), and the C2 domain (190-350), followed by the carboxy-terminal tail (CTT) including the PDZ binding motif (PDZ-BM, $^{401}$TKV$^{403}$) at the C-terminal end (Figure 1). The phosphatase domain is key in PTEN's catalytic activity with the P loop (residues 123-130) containing the catalytic signature motif, HCxxGxxR (where x is any amino acid), commonly found in the active sites of other protein tyrosine phosphatases (Denu et al., 1996; JO Lee et al., 1999). Within the motif, Cys124 is crucial

69 for transferring a phosphate group from the inositol of $PIP_3$ during the catalytic activity (Xiao et
70 al., 2007). Reversible oxidation involving disulfide formation between Cys71 and Cys124 at the
71 active site inhibits the phosphatase activity of PTEN (CU Lee et al., 2015). In the cytoplasm, PTEN
72 exists as a monomer and can even form a homodimer *in vtro* (Heinrich et al., 2015). The disordered
73 CTT is key to the regulation of the monomeric PTEN state in the cytosol through the
74 phosphorylation of the serine-threonine cluster (Ser380, Thr382, Thr383, and Ser385) located in
75 it (Bolduc et al., 2013; Masson et al., 2016; Masson and Williams, 2020; Mingo et al., 2019;
76 Vazquez et al., 2000). Cytosolic PTEN monomers exhibit a "closed-closed" conformation with
77 phosphorylated CTT ("closed" CTT covers the membrane binding interface of the phosphatase
78 and C2 domains, and "closed" PBD nestles against the phosphatase domain), and an "open-closed"
79 conformation with dephosphorylated CTT (Malaney et al., 2013; Rahdar et al., 2009; Ross and
80 Gericke, 2009) ("open" CTT exposes the membrane binding interface of the phosphatase and C2
81 domains). The dephosphorylated CTT releases the autoinhibition in the active site, facilitating the
82 translocation of PTEN to the membrane (Nussinov et al., 2020). At the membrane, PTEN yields
83 an "open-open" conformation, finally releasing its PBD. Experimental data indicated that
84 electrostatic interactions between the positively charged residues in the PBD and the C2, and the
85 negatively charged anionic lipids play a crucial role in the recruitment of PTEN to the membrane
86 (Denning et al., 2007; Nguyen et al., 2014b; Walker et al., 2004). In particular, the short N-terminal
87 PBD is important for controlling PTEN membrane localization. This established description has
88 provided a useful phenomenological overview of PTEN. However, the mechanistic details of the
89 membrane association, membrane-bound conformations and catalytic conformational changes of
90 PTEN at atomic resolution, critical for gaining functional insight into the workings of this tumor
91 suppressor and possible new venues for drug discovery, are still unknown.

92 Here, we aim to provide such mechanistic understanding of PTEN at the membrane. Our
93 study is extensive. We performed explicit solvent MD simulations on full-length, wild-type PTEN
94 interacting with lipid bilayers. The bilayer systems mainly consist of zwitterionic, 1,2-dioleoyl-sn-
95 glycero-3-phosphocholine (DOPC) and anionic, 1,2-dioleoyl-sn-glycero-3-phosphoserine (DOPS)
96 lipids. In addition, the signaling phosphatidylinositols, $PIP_2$, and $PIP_3$, were added as described in
97 Table 1. The initial conformation of PTEN at the membrane is the "open-closed" conformation
98 with dephosphorylated CTT. Dephosphorylation of CTT uncovers the active site in the
99 phosphatase domain, permitting PTEN to exert its catalytic function targeting $PIP_3$ in the
100 membrane (Nussinov et al., 2020). In our studies, PTEN stably anchored in the anionic membrane
101 with both signaling lipids, and with the two positively charged loops, one from the phosphatase
102 domain and the other from the C2 domain, inserted into the amphipathic interface of the lipid
103 bilayer. Remarkably, PTEN evolved into the "open-open" conformation spontaneously releasing
104 the PBD from the phosphatase domain to nearby $PIP_2$ in the membrane. The additional anchor by
105 PBD added to the stability of PTEN membrane association. Effective membrane localization is
106 crucial for PTEN to exert its lipid phosphatase activity, which leads to the inhibitory effect on
107 signaling via the PI3K/AKT/mTOR pathway. Our studies identify the detailed mechanisms
108 deciphering atomistic interactions of how PTEN anchors to the membrane and elucidate the vital
109 mechanistic role of PTEN in restraining cancer.
110

111 ## Results

112 ### PBD targets $PIP_2$ via conformational change and membrane localization

113 MD simulations were performed on full-length PTEN interacting with an anionic lipid bilayer
114 composed of DOPC, DOPS, $PIP_2$, and $PIP_3$ lipids (PI system, Table 1). The anionic bilayer system

115 was constructed through random distribution of the anionic lipids on the plane of the bilayer,
116 except $PIP_3$ which was placed nearer the protein. PTEN was initially placed on the lipid bilayer
117 with its putative membrane-binding interface facing toward the bilayer surface as suggested by the
118 crystal structure (JO Lee et al., 1999). An asymmetric profile of electron density across the bilayers
119 indicates that the placement of the protein depletes the electron density due to the volume occupied
120 by the bulky waters (Figure 2–figure supplement 1A). In the profile, the distance between two
121 peaks determines the bilayer thickness. The initial configuration of the PTEN-bilayer system
122 ensures that the phosphatase and C2 domains are placed on the top of the bilayer surface without
123 inserting the protein backbone into the bilayer. In this initial configuration, both the PBD and the
124 C-tail do not directly interact with the lipid bilayer (Figure 2–figure supplement 1B). However,
125 during the simulation, we observed that PTEN gradually diffuses into the bilayer and fully relaxed
126 in the lipid environment (Figure 2A). The full relaxation process for the PTEN-bilayer system
127 requires several hundred nanoseconds, which is comparatively longer than that for the protein-
128 bulky water system. For most of the anionic bilayer systems (PS, P2, P3, and PI systems, defined
129 in Table 1), we observed that the equilibrations were generally reached at ~400 ns. For PTEN in
130 the PI system, the phosphatase domain retains its structural integrity with averaged root-mean-
131 squared-deviation (RMSD) of 1.7 ± 0.2 Å with respect to the starting point. While the C2 domain
132 preserves a β-sandwich structure, its RMSD increases to 4.4 ± 0.9 Å due to fluctuations in the
133 unstructured IDR (intrinsically disordered region; residues 282-312). Large fluctuations are
134 prominent in the unstructured regions including the C-terminal region as observed in the residual
135 RMS-fluctuations (Figure 2B). Of interest is the large conformational change of PBD. The initial
136 α-helical motif in PBD is rapidly disrupted and converted into an unstructured chain (Figure 2–
137 figure supplement 1C). Interestingly, after ~400 ns, the unstructured PBD spontaneously docks

138 onto the bilayer surface establishing a secure anchor point for the phosphatase domain in the
139 membrane (Figure 2C). The membrane anchorage of PBD is sustained by strong salt bridge
140 interactions between the anionic lipids and the polybasic patch (Arg11, Lys13, Arg14, and Arg15),
141 resulting in the coordination of two $PIP_2$ lipids (Figure 2D). The N-terminus residue Met1 diffuses
142 into the hydrophobic core of the lipid bilayer, inducing nearby Lys6 to localize at the amphipathic
143 interface of the bilayer and to interact with a phosphate group of DOPC. Although our RMS-
144 fluctuations data show that PBD has large fluctuations due to the conformational change and the
145 membrane translocation, the dipping of the N-terminus in the bilayer reduces these fluctuations,
146 thus enhancing the stability of the PTEN membrane interaction following completion of the PBD
147 anchorage.
148

149 **Membrane localizing PTEN is highly sensitive to lipid composition**

150 PTEN targets the substrate lipid $PIP_3$ and co-localizes with it. The substrate is found in the inner
151 leaflet of $PIP_3$-rich microdomain within the plasma membrane. Thus, precise PTEN membrane
152 localization on the substrate is crucial for exerting its lipid phosphatase activity. To decipher how
153 PTEN is effectively absorbed in the membrane in the presence/absence of the substrate,
154 simulations were performed for PTEN with various lipid compositions in the bilayers as outlined
155 in Table 1. To derive results from the lipid effects, the same PTEN as in the PI system (Figure 2–
156 figure supplement 1B) was applied for all bilayer systems, ensuring that all starting points have
157 the same initial membrane orientation and location for the protein. To identify membrane binding
158 sites, the probability distribution functions of membrane contacts were measured as a function of
159 the protein residues (Figure 3). Remarkably, for PTEN in the zwitterionic DOPC bilayer (PC
160 system), the phosphatase domain loses contacts with the membrane (Figure 3–figure supplement

161 2A). The low probability of membrane contacts for both PBD and phosphatase domain indicates
162 the loss of the contacts. The phosphatase domain is highly elevated from the bilayer surface (Figure
163 3–figure supplement 2B), while the C2 domain is still attached to the bilayer, which prevents entire
164 protein domains from flipping on the bilayer surface. However, in the presence of anionic DOPS
165 lipid (PS system), PTEN regains its ability toward membrane attachment. Six loops located in the
166 phosphatase and C2 domains are responsible for the membrane association. These are PBD-pβ1
167 ($_{19}$DGFDL$_{23}$), pβ2-pα1 (aka Arginine loop, $_{41}$RLEGVYR$_{47}$), and pα5-pα6 (aka TI loop,
168 $_{161}$RDKKGV$_{166}$) loops in the phosphatase domain, and cβ1-cβ2 ($_{205}$MFSGGTC$_{211}$), CBR3
169 ($_{260}$KQNKMLKKDK$_{269}$), and Cα2 (aka Motif 4, $_{327}$KANKDKANR$_{335}$) loops in the C2 domain.
170 Among these, the pβ2-pα1, CBR3, and Cα2 loops were identified as membrane-binding regulatory
171 interfaces in PTEN (Nguyen et al., 2014a; Nguyen et al., 2014b). In particular, the Lys-rich CBR3
172 loop is known as the phosphatidylserine binding motif for the C2 domain (Huang et al., 2012; JO
173 Lee et al., 1999). In the P2 system with the addition of $PIP_2$, PTEN still conserves all six loop
174 regions for the membrane contact. However, in the P3 system with the addition of $PIP_3$, the TI
175 loop completely loses the membrane contact. The same behavior is also observed for the TI loop
176 in the PI system with the addition of both signaling lipids, $PIP_2$ and $PIP_3$ (Figure 3, bottom panel).
177 Moreover, the Cα2 loop weakens the membrane contacts. For the TI loop, the loss of the membrane
178 contacts is closely related to the presence of $PIP_3$, while it is related to the presence of $PIP_2$ for the
179 Cα2 loop. These signaling lipids move into the region underneath the interface between the
180 phosphatase and C2 domains, bolstering PTEN on the membrane. Especially, the interaction of
181 $PIP_3$ with the phosphatase domain yields a distinct membrane orientation for the domain. We
182 observed that $PIP_3$-containing P3 and PI systems generate a similar profile of the distributions of
183 the helix tilt angles for the helices in the phosphatase domain (Figure 3–figure supplement 3).

184 Unlike the phosphatase domain, the C2 domain retains its membrane binding sites for all anionic
185 bilayer systems, indicating its intrinsic feature that targets cell membrane.

186 The presence of $PIP_3$ also affects the conformation of PBD. While the PBD retains the
187 initial α-helical motif in the PC and PS systems, it is partially unfolded in the P2 system (Figure
188 3–figure supplement 2A) and completely denatured in the P3 system (Figure 3–figure supplement
189 4A). The unfolding of PBD is also observed in the PI system (Figure 2–figure supplement 1C),
190 suggesting that only P3 and PI systems contain $PIP_3$. In the P3 system, the unfolded PBD emerges
191 at ~350 ns, which is relatively longer than the PI system with ~40 ns. We observed abrupt changes
192 in the deviation of the center of mass of PBD from the bilayer surface, indicating that the N-
193 terminus flips the location back and forth with respect to the phosphatase domain (Figure 3–figure
194 supplement 4B). In the first flip event, the PBD failed to secure the interaction with the membrane
195 due to unavailability of anionic lipids at the flipping site. However, in the presence of anionic
196 lipids near the PBD binding site, the polybasic motif $_{11}$RNKRR$_{15}$ is able to interact with DOPS
197 as in the PS system (Figure 3–figure supplement 4C) and $PIP_2$ as in the P2 system (Figure 3–figure
198 supplement 4D) even though both systems have the folded α-helical PBD sequestered by the
199 phosphatase domain. We found that among the polybasic residues in PBD, Lys13 and Lys14
200 appeared to be key residues interacting with anionic lipids. It was reported that K13E mutation
201 impairs the ability of PTEN to bind anionic lipid bilayer (Walker et al., 2004).

202

203 **Strong salt bridge interactions between key basic residues and**
204 **phosphatidylinositol lipids conduce PTEN membrane localization**

205 To corroborate the effects of phosphatidylinositol lipids on the membrane localization of PTEN,
206 we trace the interactions of basic residues in both phosphatase and C2 domains. PTEN contains a

207 high population of basic residues (Arg and Lys) at the membrane binding interface, 29 out of the
208 total 54 basic residues participate in the interaction with lipids. These basic residues are mainly
209 located at the PBD and the loop regions in the phosphatase and C2 domains, forming salt bridges
210 with the phosphate group of the lipids and the head groups of the anionic lipids. Both the PBD and
211 phosphatase domain are Arg-rich, while the C2 domain is Lys-rich (Figure 4A). The high
212 probability of forming salt bridges indicates that Arg favors $PIP_2$, while Lys favors $PIP_3$ (Figure
213 4B). Those Arg residues, Arg14 (in PBD), Arg161 (in phosphatase), and Arg335 (in C2) exhibited
214 high probability in forming salt bridges with $PIP_2$ (Figure 4–figure supplement 5A). In contrast,
215 those Lys residues, Lys125, Lys128, and Lys164 in the phosphatase domain, and Lys221, Lys223,
216 Lys267, Lys269, and Lys330 in the C2 domain exhibited high probability of forming salt bridges
217 with $PIP_3$. While $PIP_2$-favored Arg residues are located proximal to the bilayer, $PIP_3$-favored Lys
218 residues including a key Arg residue, Arg130, are located distal to the bilayer surface. Basic
219 residues with high probability in forming salt bridges with $PIP_3$ have large deviations from the
220 bilayer surface (Figure 4C), suggesting that $PIP_3$ favors distal basic residues in the salt bridge
221 interactions. Such basic residues, Lys125, Lys128, and Arg130 can be found in P loop, which is
222 located at ~15 Å, largely elevated from the bilayer surface. In the salt bridge interactions with
223 DOPC and DOPS, the basic residues exhibit a similar pattern (Figure 4–figure supplement 5B),
224 indicating that salt bridges occurred with high probability for those basic residues at the loop
225 regions inserted into to the amphipathic interface of the lipid bilayer. These are the pβ2-pα1 and
226 CBR3 loops in the phosphatase and C2 domains, respectively. In this case, the basic residues can
227 be located close to the bilayer surface being able to form salt bridges with the phosphate and acidic
228 head groups of bulky lipids. Arg41 in the pβ2-pα1 loop strongly interacts with the lipids as
229 observed in the experiments (Nguyen et al., 2014b). The CBR3 loop in the C2 domain is embedded

230 in the amphipathic interface of the lipid bilayer, promoting its basic residues to form salt bridges
231 with DOPS with relatively high probability as compared to other anionic lipids.
232

233 **Substrate coordination and conformational change of P loop implicate PTEN**
234 **catalytic activity**

235 In the lipid phosphatase activity of PTEN, the P loop at the active site plays a significant role in
236 transferring a phosphate group from $PIP_3$ substrate. To recruit the substrate lipid, the P loop needs
237 to extract it from the bilayer, since the loop is located highly distal to the bilayer surface. Our data
238 illustrate that $PIP_3$ significantly protrudes from the bilayer surface and repositions toward the
239 active site (Figure 5A). The protruding $PIP_3$ can form salt bridges with key basic residues in P
240 loop. Deviations of the lipids from the bilayer surface show prominent protrusions of the lipids in
241 the *holo* membrane side containing the protein as compared to those in the *apo* membrane side
242 (Figure 5B). Note that $PIP_2$ in *holo* also shows a weak protrusion but less significantly than $PIP_3$,
243 since $PIP_2$ pursues the basic residues of PBD that reside in the bilayer surface. No significant
244 protrusions of the phosphatidylinositol lipids can be observed for the monotonic systems
245 containing only $PIP_2$ (P2 system) or $PIP_3$ (P3 system) (Figure 5–figure supplement 6A). This
246 indicates that the P2 system is deficient in $PIP_3$, and the P3 system fails to recruit $PIP_3$ to the active
247 site. In the PTEN phosphatase domain, the P loop contains the catalytic signature motif
248 $_{123}$HCKAGKGR$_{130}$ that is characteristic of the active site of the phosphatase family (JO Lee et
249 al., 1999). It is important for Arg130 to coordinate $PIP_3$ in the catalytic activity, since Arg130
250 facilitates migration of a phosphate group from the inositol head of $PIP_3$ to the sidechain of Cys124.
251 In addition to the catalytically significant Arg130, we discovered that two Lys residues, Lys125
252 and Lys128 in the P loop also coordinate $PIP_3$. These Lys residues are PTEN-specific. In the P

253 loop, two $PIP_3$ are observed in the coordination; one with Lys128 and the other with Lys125 and
254 Arg130. The $PIP_3$ coordination changes the P loop to an "open" conformation with the
255 rearrangement of the sidechains of the catalytic residues, Cys124 and Arg130, toward the substrate
256 (Figure 5C). In the crystal structure of PTEN, the P loop shows a "collapsed" conformation (Figure
257 5–figure supplement 6B). In our simulations, the P loop retains the collapsed conformation in the
258 PS, P2, and P3 systems (Figure 5–figure supplement 6C). The PS and P2 systems lack $PIP_3$ in the
259 bilayers, but the P3 system retains it. We found that the P3 system fails to coordinate $PIP_3$ to
260 Arg130 in the active site. The failure of the coordination of $PIP_3$ to Arg130 is also observed in the
261 one of PI systems in which the P loop retains the collapsed conformation. In the PI systems with
262 the $PIP_3$ coordination, the sidechain of Asp92 in the WPD loop (residues 88-98) is rotated to the
263 binding site, appearing to participate in the catalytic activity (Figure 5C and Figure 5–figure
264 supplement 6D). This further implicates the "closed" WPD loop conformation with high catalytic
265 activity (Brandao et al., 2012; Chia et al., 2010). However, studies of Asp92 mutations *in vivo* and
266 *in vitro* suggested that Asp92 residue is not a catalytic amino acid commonly involved in the
267 hydrolysis of $PIP_3$ by PTEN (Rodriguez-Escudero et al., 2011).

268 In PTEN, the phosphatase and C2 domains are hinged by a short linker, $_{186}$LDYR$_{189}$,
269 located far from the bilayer surface. Underneath the linker, there is a cave-like, water-filled space
270 encompassed by these two domains and the bilayer surface, serving as an aqueous canal (Figure
271 6A). Through this region, aqueous molecules can penetrate the active site. Also, $PIP_3$ with large
272 inositol head can enter the region from both ends and move to the active site along the path
273 connecting the $PIP_3$-favored distal basic residues. The HOLE program (Smart et al., 1993)
274 calculated the structure of aqueous canal, illustrating that the canal with the dimension is large
275 enough for water transport (Figure 6B). Catalytic activity requires the water molecules for

276 hydrolysis to release the phosphate group from Cys124 after transferring it from $PIP_3$. Three-
277 dimensional water density map illustrates high populations of residual waters around the
278 sidechains of Cys124 and Arg130 at the active site (Figure 6C). The high probability of water
279 suggests that the lipid substrate transports water molecules that soak the active site. In contrast,
280 density maps with less waters populating the sidechains of catalytic residues in the P loop can be
281 observed in the active sites of systems where $PIP_3$ is absent (Figure 6–figure supplement 7). Due
282 to formation of the water-filled space, no significant interdomain interaction between the
283 phosphatase and C2 domains is observed (Figure 6D). However, the high residue-residue contact
284 probability indicates that the phosphatase residues Ser170 and Arg173 tightly hold the
285 phosphatase–C2 domain interface underneath the short linker. Oncogenic mutations abolishing
286 this interface (Smith et al., 2019) commonly occur at the interface residues Ser170 and Arg173,
287 resulting in inactivation of PTEN in cancer (JO Lee et al., 1999). The N-terminal PBD marginally
288 contacts the phosphatase domain, while the CTT largely contacts the phosphatase and C2 domains.
289

290 **Conformations of the IDR in the C2 domain and CTT in the C-terminal region**

291 The IDR was initially unstructured, and most of the region in the domain remained disordered as
292 it was. However, the segment $_{306}$IER$_{308}$ participates in the β-sheet formation with cβ7 strand
293 (Figure 6–figure supplement 8A). The β-sheet extension is stable as observed for most PTEN
294 systems. Occasionally, the segment $_{299}$EIDSIC$_{304}$ folds into an α-helix as calculated by STRIDE
295 (Frishman and Argos, 1995) (Figure 6–figure supplement 8B), but most PTEN systems display it
296 as a turn conformation. In contrast, the CTT retains the unstructured characteristics with large
297 fluctuations in most PTEN systems. Its conformational space spans from a collapsed chain with
298 radius gyration $R_g$ = ~15.0 Å to an extended chain with $R_g$ = ~24.0 Å (Figure 6–figure supplement

299 8C). The long unstructured CTT chain can reach the phosphatase domain as shown in the residue-
300 residue contact map (Figure 6C), while the collapsed CTT mainly rides on the C2 domain. Thus,
301 the interaction of CTT with the phosphatase and C2 domains are highly dynamic due to the various
302 conformational ensembles. As observed in previous computational studies (Shenoy et al., 2012),
303 no membrane interaction of CTT was observed, suggesting that the CTT does not interfere in the
304 PTEN membrane localization and $PIP_3$ recruitment by the phosphatase domain.
305

306 ## Discussion

307 We report here selective membrane interaction of PTEN in the absence and presence of the
308 signaling lipids phosphatidylinositol $PIP_2$ and $PIP_3$. The canonical role of PTEN is to negatively
309 regulate the PI3K/AKT/mTOR pathway by dephosphorylating the lipid substrate $PIP_3$ into $PIP_2$.
310 PTEN targets distinct membrane microdomains that are enriched in phosphatidylinositol lipids.
311 Our studies demonstrate that effective membrane localization of PTEN depends on the lipid
312 composition in the membranes. We mimic several types of microdomains within the plasma
313 membrane (Table 1). In the zwitterionic membrane, PTEN abrogates its catalytic activity
314 impairing the interaction of the phosphatase domain with the membrane, while the C2-membrane
315 interaction remains intact. In the presence of phosphatidylserine, PTEN proceeds with membrane
316 localization through the docking of the pβ2-pα1 loop of the phosphatase domain into the anionic
317 membrane. The C2 domain conserves its intrinsic feature targeting the cell membrane through the
318 insertion of the CBR3 loop into both zwitterionic and anionic membranes. A series of basic Lys
319 residues in the CBR3 loop buttress the interaction of PTEN with the anionic membrane containing
320 phosphatidylserine. The process of PTEN membrane localization is completed through the stable
321 anchorage of the unstructured PBD in the anionic membrane containing both phosphatidylinositols,

322 $PIP_2$ and $PIP_3$ (Figure 7), suggesting that full activation of PTEN requires both lipids interacting
323 with the specific domains; $PIP_3$ at the active site and $PIP_2$ at the PBD binding site. We suggest that
324 the coordination of $PIP_3$ to the P loop in the active site of the phosphatase domain can allosterically
325 induce PBD unfolding. Once the unfolded PBD recognizes $PIP_2$ at the binding site, it is released
326 from the phosphatase domain and translocated onto the membrane surface. Taken together, PTEN
327 uses three major anchor points, the N-terminal PBD, the pβ2-pα1 loop in the phosphatase domain,
328 and the CBR3 loop in the C2 domain to maintain the stable membrane-interacting conformation.

329 Previous computational studies indicate that electrostatic interactions initially drive PTEN
330 to the membrane, followed by reorientation of the protein to optimize its interactions with the
331 substrate (Kalli et al., 2014; Lumb and Sansom, 2013; Shenoy et al., 2012). Our data indicate that
332 the salt bridge interactions between the basic residues and the lipids are a major driving force in
333 stabilizing the protein-membrane interface. These basic residues are in the three major anchor
334 points among the domains, located close to the membrane surface with the proximal basic residues
335 forming salt bridges with the phosphate atom of the head groups of phosphatidylcholine and
336 phosphatidylserine. In contrast, the basic residues distal to the membrane are positioned at the
337 water-filled interface between the phosphatase and C2 domains. The cave-like, water-filled space
338 formed by the inner surfaces of these domains and the membrane surface denotes the aqueous
339 canal. The distal basic residues including the catalytically significant Lys125, Lys128, and Arg130
340 in the P loop, are closely associated with $PIP_3$ migration towards the active site. Lys125
341 occasionally coordinates $PIP_3$ with Arg130, suggesting its auxiliary role in the catalysis, and
342 Lys128 has high probability of $PIP_3$ binding. Other distal basic residues in the aqueous canal may
343 pave the road for the substrate lipid to move toward the active site, serving as a reservoir for the
344 $PIP_3$-binding sites. Furthermore, the open P loop conformation points to PTEN in the active state,

345 primed for catalysis. Importantly, mutations and acetylation of Lys125 and Lys128 results in a
346 reduction of PTEN phosphatase activity (JO Lee et al., 1999; Okumura et al., 2006) further
347 demonstrating their critical role in catalysis. Overall, observations of $PIP_3$ coordination at Cys124
348 and Arg130, the proximity of Asp92 in the WPD loop to the coordination, and the high population
349 of the residual waters at the active site suggest that these events participate in cooperative catalysis.

350 Previous PTEN studies showed that affinity to the membrane is reduced by the following:
351 cancer-associated mutations (Masson and Williams, 2020) inhibit recruitment to the plasma
352 membrane, thus abolishing its interactions with phospholipids (Nguyen et al., 2015);
353 phosphorylation of the CTT serine-threonine cluster impairs PTEN membrane binding ability,
354 resulting in a closed protein conformation (Bolduc et al., 2013; Malaney et al., 2013; Masson and
355 Williams, 2020; Rahdar et al., 2009; Ross and Gericke, 2009); CTT deletion decreases protein
356 stability leading to tumor development (Georgescu et al., 1999; Sun et al., 2014); and a mutation
357 in the PBD (K13E) leads to PTEN inactivation (Masson and Williams, 2020; Nguyen et al., 2015;
358 Walker et al., 2004). In the cytosol, monomeric PTEN is in the inactive state with its PBD bound
359 to the phosphatase domain and the phosphorylated CTT interfering with the membrane binding
360 interface (Chen et al., 2016) (Figure 7), whereby the inactive, autoinhibited PTEN is in the "closed-
361 closed" conformation.

362 Here, we propose that in the autoinhibited PTEN conformation, the long, unstructured
363 phosphorylated CTT covers the distal basic residues positioned along the aqueous canal,
364 preventing the recruitment of the substrate. The highly negatively charged IDR at the opposite site
365 of C2 promotes the phosphorylated CTT to correctly interact with the membrane binding interface,
366 spawning the autoinhibited state. Dephosphorylation of the CTT shifts the population to the
367 membrane binding-ready, "open-closed" conformation. With the exposure of its membrane

368 binding interface, PTEN can localize on the membrane. In the absence of phosphatidylinositols,
369 the PBD is still in a closed conformation, however, PTEN acquires full activation with the "open-
370 open" conformation, when interacting with membrane microdomains enriched with
371 phosphatidylinositols. Notably, PTEN also targets the membrane microdomains that PI3K does,
372 co-localizing with its substrate, suggesting that both negative and positive regulators in the
373 PI3K/AKT/mTOR pathway concomitantly exist at the same microdomains within the plasma
374 membrane.

375 To date, PTEN has been considered clinically undruggable due to its status as a tumor
376 suppressor phosphatase and its complex regulation. A major challenge in thwarting its oncogenic
377 mutations is that PTEN is a tumor suppressor, not an activator. In other words, oncogenic PTEN
378 is inactive, and not active. Activation is dramatically more difficult to achieve than inactivation,
379 due to the diverse nature of its mutations. Nevertheless, the mechanistic details elucidated in this
380 work may suggest exploring at least two potential venues. The first relates to relieving PTEN's
381 autoinhibition, shifting from an inactive state to an active state. Though this has been previously
382 explored (Kalli et al., 2014; Lumb and Sansom, 2013), the details provided here may suggest
383 additional PTEN structural features to target. We suggest that charge reversal mutations on the
384 IDR release the autoinhibition through the interaction with the phosphorylated CTT, exposing the
385 membrane binding interface of the phosphatase and C2 domains and thus promoting membrane
386 localization of PTEN. The second relates to the design of allosteric drugs that restore the
387 coordination in PTEN mutants in which catalysis is impaired, such as the C124S mutant which is
388 catalytically dead (Bonneau and Longy, 2000), and the G129E mutation which inhibits the
389 recognition of phosphatidylinositol (Myers et al., 1998). Here we detail the substrate coordination
390 and conformational change of the P loop that implicate PTEN catalytic activity. We observed that

391 $PIP_3$ significantly protrudes from the membrane surface and can form salt bridges with key basic
392 residues in the P loop. $PIP_2$ in the *holo* state also protrudes but less significantly. Residues Cys124
393 and R130 are essential for catalysis whereby is vital for $PIP_3$ coordination, facilitating the
394 phosphate group migration from its inositol to Cys124. Lys125 and Lys128 in the P loop also
395 coordinate $PIP_3$ and are PTEN-specific. Moreover, we observed two crucial active site
396 coordination events, namely $PIP_3$ with Lys128, and Lys125 and Arg130, which alters P loop
397 conformation through sidechain rearrangement of the catalytic residues, Cys124 and Arg130,
398 toward the substrate. The use of allosteric modulators to restore these coordination events in PTEN
399 mutants can provide therapeutic advantages. One possible approach would be via the design of an
400 allostery-based rescue mutant as we have proposed for PI3Kα (Zhang et al., 2020) and earlier for
401 the von Hippel-Lindau tumor suppressor protein (Liu and Nussinov, 2008). An alternative
402 approach to overcome any mutational effects and restore wild-type PTEN function would be the
403 design of small-molecule allosteric modulators that target the allosteric communication pathway
404 from the PBD region to the active site that stabilizes PTEN–membrane interactions.

405 In conclusion, membrane localization and orientation of PTEN strongly depend on the lipid
406 composition of the membrane. Our studies elucidate the mechanistic details of PTEN activation at
407 the membrane and the role of phosphatidylinositols in the conformational changes of membrane
408 bound PTEN. Cancer-associated mutations prevent effective membrane localization, leading to
409 the dysfunctional inhibition of oncogenic cell signaling and growth. With PTEN being one of the
410 most frequently mutated proteins in cancers, obtaining its membrane associated structure and
411 mechanism in atomic resolution may provide insight assisting drug discovery, for the currently
412 still undruggable major cancer target (McLoughlin et al., 2018).

413

414 # Materials and methods

415 ## Preparing the full-length PTEN

416 The crystal structure of wild-type PTEN (PDB: 1D5R) was used to model the full-length PTEN
417 protein. The missing coordinates for residues 1-13 in PBD, residues 282-312 of IDR in C2, and
418 residues 352-403 in the CTT were obtained by a hierarchal iterative template-based threading
419 approach using the I-TASSER program (Roy et al., 2010; Yang et al., 2015; Yang and Zhang,
420 2015). The PBD was modelled as a small α-helix, and the IDR and CTT were modelled as
421 unstructured chains (Figure 1). *In silico* modelling of full-length PTEN showed that the α-helix
422 PBD interacts with the phosphatase domain and both unstructured IDR and CTT chains span the
423 phosphatase and C2 domains marginally interacting with them. We ensured that the long
424 disordered CTT chain does not block the catalytic site at the membrane binding interface. In
425 autoinhibition, the catalytic site is blocked by phosphorylated serine-threonine cluster (Ser380,
426 Thr382, Thr383, and Ser385) in the CTT, which is crucial for maintaining PTEN in a stable
427 cytosolic state (Masson and Williams, 2020).

428

429 ## Construction of the bilayer systems with PTEN

430 To generate the initial configuration of membrane bound PTEN, the protein was placed on the
431 lipid bilayer without contacting the lipids. In the initial placement, PTEN faced its putative
432 membrane-binding interface toward the bilayer surface as suggested by the crystal structure (JO
433 Lee et al., 1999). In this orientation, the pβ2-pα1 loop (residues 40-47) in the phosphatase domain
434 and the CBR3 loop (residues 260-269) in the C2 domain were closely located at the bilayer surface.
435 The initial construction revealed that all modelled regions including the N-terminal PBD do not
436 interact with the bilayer before starting of the simulations. An equilibrated and hydrated lipid

437 bilayer was constructed at the room temperature ensuring that the lipid bilayer is in the liquid
438 phase. In the construction, preequilibrated lipids from the lipid library containing a couple of
439 thousand lipids with different individual conformations generated from the CHARMM program
440 (Brooks et al., 2009) were extracted and replaced with the pseudospheres interacting through the
441 van der Waals (vdW) force field at the putative locations for the phosphate atom of lipid head
442 group (Woolf and Roux, 1994, 1996). The bilayer contained 4 different lipids including the
443 zwitterionic DOPC, anionic DOPS, and the phosphatidylinositol $PIP_2$ and $PIP_3$ lipids in 32:6:1:1,
444 molar ratio (Table 1). Total of 400 lipids constituted the bilayer system with lateral cell dimension
445 of ~120 $Å^2$ for the unit cell. TIP3P waters were added at both sides of the bilayer with lipid/water
446 ratio of ~1/130.
447

448 **Atomistic molecular dynamics simulations**

449 We performed MD simulations using the updated CHARMM (Brooks et al., 2009) all-atom force
450 field (version 36m) (Huang et al., 2017; Klauda et al., 2010) for constructing the set of starting
451 points and relaxing the systems to a production-ready stage. Our simulations closely followed the
452 same protocol as in our previous works (Chakrabarti et al., 2016; Chavan et al., 2015; Jang et al.,
453 2015; Jang et al., 2017; Jang et al., 2016a; Jang et al., 2019; Jang et al., 2016b; Jang et al., 2020;
454 Liao et al., 2018; Liao et al., 2017; Lu et al., 2015; Lu et al., 2016; Muratcioglu et al., 2017;
455 Ozdemir et al., 2018a; Ozdemir et al., 2018b; Zhang et al., 2017; Zhang et al., 2019a, 2019b). The
456 bilayer system containing PTEN and solvent has almost 210,000 atoms. For reproducibility, we
457 constructed four independent systems with different lipid arrangements around protein. Statistics
458 were taken over these trajectories. To observe the effects of lipid compositions on the PTEN-
459 membrane interaction, four additional systems were constructed, including a pure DOPC bilayer,

460 an anionic DOPC:DOPS (4:1, molar ratio) bilayer, and two anionic DOPC:DOPS:$PIP_2$ and
461 DOPC:DOPS:$PIP_3$ bilayers in 16:3:1, molar ratio (Table 1). The former and latter
462 phosphatidylinositol lipid bilayers radically contained $PIP_2$ and $PIP_3$, respectively.

463 In the preequilibrium stage, we performed a series of minimization and dynamics cycles
464 for the solvents including lipids around the harmonically restrained protein. Each bilayer system
465 was subjected to the preequilibrium simulation for 5 ns with the restrained backbones of PTEN
466 until the solvent reached 310 K. The harmonic restraints on the backbones of PTEN were gradually
467 removed through the solvent dynamics cycles with the particle mesh Ewald (PME) electrostatics
468 calculation (Darden et al., 1993). The final dynamics cycle without the harmonic restraints
469 completed the preequilibrium stage, generating the starting point for the production run. A total of
470 8.0 μs simulations were performed for the 8 systems, each with 1 μs. In the production runs, we
471 employed the Langevin temperature control (Wu and Brooks, 2003) to maintain the constant
472 temperature at 310 K and the Nosé-Hoover Langevin piston pressure control to sustain the pressure
473 at 1 atm. To constrain the motion of bonds involving hydrogen atoms, we applied the SHAKE
474 algorithm (Ryckaert et al., 1977). The production runs were implemented with the NAMD parallel-
475 computing code (Phillips et al., 2005) on a Biowulf cluster at the National Institutes of Health
476 (Bethesda, MD). In the analysis, the first 200 ns trajectories were removed, and thus averages were
477 taken afterward.
478

479 **Table 1** Composition of the lipid bilayer systems in the simulations.
480

| System | Charged state | # of DOPC | # of DOPS | # of $PIP_2$ | # of $PIP_3$ | Molar ratio |
|---|---|---|---|---|---|---|
| **PC** | Zwitterionic | 400 | - | - | - | 1 |
| **PS** | Anionic | 320 | 80 | - | - | 4:1 |
| **P2** | Anionic | 320 | 60 | 20 | - | 16:3:1 |
| **P3** | Anionic | 320 | 60 | - | 20 | 16:3:1 |
| **PI** | Anionic | 320 | 60 | 10 | 10 | 32:6:1:1 |

481
482

483 ## Figure legends

484

485 **Figure 1.** PTEN sequence and structure.

486 (A) The sequence and domain structure of PTEN. In the sequence, the underlined residues
487 highlight the $PIP_2$ binding domain (PBD) at the N-terminal and the PDZ binding motif at
488 the C-terminal regions. In the domain structure, the phosphorylated serine-threonine cluster
489 (residues 380-385) in the C-terminal tail is marked.

490 (B) The crystal structures of PTEN (PDB code: 1D5R). The marked residues denote the
491 missing regions.

492 (C) *In silico* model of the full-length PTEN structure. The missing regions in PTEN, the PBD
493 (residues 1-15), the interdomain region (IDR, residues 282-312), and the C-terminal tail
494 (residues 351-403) were constructed by the I-TASSER program (Roy et al., 2010; Yang et
495 al., 2015; Yang and Zhang, 2015).

496

497 **Figure 2.** Membrane interaction of PTEN.

498 (A) Snapshot representing the final PTEN conformation in the lipid bilayer composed of
499 DOPC:DOPS:$PIP_2$:$PIP_3$ = 32:6:1:1, in molar ratio.

500 (B) The root-mean-squared-fluctuations (RMSFs) of PTEN residues.

501 (C) Time series of the deviations of the center of mass of individual PTEN domains from the
502 bilayer surface.

503 (D) Highlight shown the interaction of unfolded PBD with the lipids. Key basic residues, Lys6,
504 Arg11, Lys13, Arg14, and Arg15 are marked.

505

506 **Figure 3.** Lipid contact probability.

507 The probability of lipid contacts for PTEN residues for different bilayer systems, including PC
508 (pure DOPC), PS (DOPC:DOPS = 4:1, molar ratio), P2 (DOPC:DOPS:$PIP_2$ = 16:3:1) , P3
509 (DOPC:DOPS:$PIP_3$ = 16:3:1) and PI (DOPC:DOPS:$PIP_2$:$PIP_3$ = 32:6:1:1) systems.

510

511 **Figure 4.** Salt bridge interactions of PTEN.

512 (A) Mapping of the basic residues on the membrane-binding surface of the phosphatase and
513 C2 domains. $PIP_3$-favored residues in the phosphatase domain are colored red, and those
514 in the C2 domain are colored blue.

515 (B) Contour map of the probabilities of salt bridge formations between the key basic residues
516 at the membrane-binding interface and the lipids. Salt bridge is calculated between the
517 nitrogen atoms in the sidechains of basic residues and the oxygen atoms in the phosphate
518 group of all lipids and the inositol head group of phosphatidylinositols with the cutoff
519 distance of 3.2 Å.

520 (C) Averaged deviations of the amide nitrogen in the sidechains of Arg and Lys residues from
521 the bilayer surface for the $PIP_3$-favored residues in the phosphatase (left panel) and C2
522 (right panel) domains.

523

524 **Figure 5.** $PIP_3$ coordination induces the P loop conformational change.

525 (A) A snapshot highlighting P loop and protruded $PIP_3$ from the bilayer surface at the active
526 site.

527 (B) Deviations of the phosphate atoms of $PIP_2$ and $PIP_3$ from the averaged position of the
528 phosphate atoms of DOPC and DOPS for the *apo* and *holo* bilayer leaflets in the absence
529 and presence of the protein, respectively.
530 (C) The open conformation of P loop with the coordination of $PIP_3$ at the active site.
531
532 **Figure 6.** High density of waters at the active site for catalysis.
533 (A) Highlight shown the cave-like, water-filled space formed by the inner surfaces of
534 phosphatase and C2 domains and the bilayer surface denoting as the aqueous canal. Along
535 the water-filled interface between the phosphatase and C2 domains, $PIP_3$-favored distal
536 basic residues are marked.
537 (B) The structure and diameter of aqueous canal calculated with HOLE program (Smart et al.,
538 1993). For the canal structure, green denotes the diameter in the range, $4 \leq d \leq 10$ Å, and
539 blue denotes the diameter of $d > 10$ Å.
540 (C) Three-dimensional water density map with probabilities, $p = 0.5$ (yellow surface) and $p =$
541 0.4 (blue mesh).
542 (D) Interdomain residue-residue contacts for PTEN. For two intramolecular residues $i$ and $j$,
543 the probability of contact for the distance between the $C_\beta^i - C_\beta^j$ ($C_\alpha$ is used for Gly residue)
544 with cutoff 10 Å was calculated. Residue $j$ with $|j - i| < 4$ was omitted, and $p < 0.1$ was
545 neglected in the calculation.
546
547 **Figure 7.** A schematic diagram illustrating membrane localization of PTEN.
548 In the cytosol, PTEN is autoinhibited by the phosphorylated CTT, through the "closed-closed"
549 conformation. Dephosphorylation on the CTT removes the autoinhibition, shifting the

550 populations toward the "open-closed" conformation. With the exposed membrane-binding
551 surface, PTEN can localize at the anionic membrane. Full activation of PTEN requires the
552 membrane anchorage of PBD at the membrane microdomain enriched by both
553 phosphatidylinositols, $PIP_2$ and $PIP_3$. In the cartoon, PTP denotes the phosphatase domain.
554

555 ## Figure supplement legends

556

557 **Figure 2–figure supplement 1.** Initial configuration of the PTEN-membrane system.

558 (A) Electron density across the bilayers for the pure DOPC bilayer (gray line) and the PI
559 system (black line) with the lipid composition of DOPC:DOPS:$PIP_2$:$PIP_3$ = 32:6:1:1, in
560 molar ratio.

561 (B) A snapshot representing the initial conformation of PTEN in the PI system.

562 (C) Time-evolution structures of PBD in the PI system. In the cartoons, hydrophobic,
563 polar/glycine, positively charged, and negatively charged residues are colored white, green,
564 blue, and red, respectively.

565

566 **Figure 3–figure supplement 2.** Relaxed PTEN conformations in different lipid bilayer systems.

567 (A) Snapshots representing the final conformations of PTEN in the PC, PS, P2, and P3 systems.

568 (B) Averaged deviations of the center of mass of individual PTEN domains from the bilayer
569 surface for different bilayer systems.

570

571 **Figure 3–figure supplement 3.** Helix tilt angle of PTEN.

572 Probability distribution functions of the helix tilt with respect to the bilayer normal for helices
573 in the phosphatase domain of PTEN in different bilayer systems.

574

575 **Figure 3–figure supplement 4.** Conformational dynamics of PBD in different bilayer systems.

576 (A) Time-evolution structures of PBD in the P3 system. In the cartoons, hydrophobic,
577 polar/glycine, positively charged, and negatively charged residues are colored white, green,
578 blue, and red, respectively.
579 (B) Time series of the deviations of the center of mass of PBD in the P3 system compared to
580 that in the PI system.
581 (C) Highlights shown the interactions of folded PBDs with the lipids in the PS system.
582 (D) The same for the P2 system. Key basic residues, Lys6, Arg11, Lys13, Arg14, and Arg15
583 are marked.
584
585 **Figure 4–figure supplement 5.** Salt bridge interactions of key basic residues.
586 (A) Two-dimensional bar graphs with error bars of the probabilities of salt bridge formation
587 between the key basic residues at the membrane-binding interface and
588 phosphatidylinositols, $PIP_2$ and $PIP_3$.
589 (B) The same for bulky lipids, DOPC and DOPS. Salt bridge is calculated between the
590 nitrogen atoms in the sidechains of basic residues and the oxygen atoms in the phosphate
591 group of all lipids and the inositol head group of phosphatidylinositols with the cutoff
592 distance of 3.2 Å.
593
594 **Figure 5–figure supplement 6.** Conformational change of P loop in different bilayer systems.
595 (A) Deviations of the phosphate atoms of $PIP_2$ in the P2 system and $PIP_3$ in the P3 system
596 from the averaged position of the phosphate atoms of DOPC and DOPS for the *apo* and
597 *holo* bilayer leaflets in the absence and presence of the protein, respectively.
598 (B) A snapshot representing the P loop conformation in the crystal structure.

599 (C) Snapshots representing the collapsed P loop conformations observed in the PS, P2, P3,
600 and $PI^4$ systems. One of the PI systems yields the collapsed P loop due to failure of the
601 coordination of $PIP_3$ to Arg130.
602 (D) Snapshots representing the open conformation of P loop with the coordination of $PIP_3$ at
603 the active site for the PI systems.
604
605 **Figure 6–figure supplement 7.** Density of waters at the active site in different bilayer systems.
606 Three-dimensional water density map with probabilities, $p = 0.5$ (yellow surface) and $p = 0.4$
607 (blue mesh) for the PS, P2, and P3 systems.
608
609 **Figure 6–figure supplement 8.** Conformations of IDR and CTT.
610 (A) Snapshot of the IDR conformation with the β-sheet extension.
611 (B) Descriptions of the secondary structure by the STRIDE program (Frishman and Argos,
612 1995) for the IDR depicted each 100 ns interval.
613 (C) Representative conformations of the CTT with the collapsed and extended chain structures.
614
615

**Acknowledgements**. This study was funded, in part, by the Ambrose Monell Foundation (to C.E.). This project has been funded in whole or in part with federal funds from the National Cancer Institute, National Institutes of Health, under contract HHSN26120080001E. The content of this publication does not necessarily reflect the views or policies of the Department of Health and Human Services, nor does mention of trade names, commercial products, or organizations imply endorsement by the U.S. Government. This Research was supported [in part] by the Intramural Research Program of the NIH, National Cancer Institute, Center for Cancer Research. All simulations had been performed using the high-performance computational facilities of the Biowulf PC/Linux cluster at the National Institutes of Health, Bethesda, MD (https://hpc.nih.gov/).

626 ## References

627


628 Alvarez-Garcia V, Tawil Y, Wise HM, Leslie NR. 2019. Mechanisms of PTEN loss in cancer:
629 It's all about diversity. *Semin Cancer Biol,* **59**:66-79.
630 doi:10.1016/j.semcancer.2019.02.001
631 Bolduc D, Rahdar M, Tu-Sekine B, Sivakumaren SC, Raben D, Amzel LM, Devreotes P, Gabelli
632 SB, Cole P. 2013. Phosphorylation-mediated PTEN conformational closure and
633 deactivation revealed with protein semisynthesis. *Elife,* **2**:e00691.
634 doi:10.7554/eLife.00691
635 Bonneau D, Longy M. 2000. Mutations of the human PTEN gene. *Hum Mutat,* **16**:109-122.
636 doi:10.1002/1098-1004(200008)16:2<109::AID-HUMU3>3.0.CO;2-0
637 Brandao TA, Johnson SJ, Hengge AC. 2012. The molecular details of WPD-loop movement
638 differ in the protein-tyrosine phosphatases YopH and PTP1B. *Arch Biochem Biophys,*
639 **525**:53-59. doi:10.1016/j.abb.2012.06.002
640 Brooks BR, Brooks CL, 3rd, Mackerell AD, Jr., Nilsson L, Petrella RJ, Roux B, Won Y,
641 Archontis G, Bartels C, Boresch S, Caflisch A, Caves L, Cui Q, Dinner AR, Feig M,
642 Fischer S, Gao J, Hodoscek M, Im W, Kuczera K, Lazaridis T, Ma J, Ovchinnikov V,
643 Paci E, Pastor RW, Post CB, Pu JZ, Schaefer M, Tidor B, Venable RM, Woodcock HL,
644 Wu X, Yang W, York DM, Karplus M. 2009. CHARMM: the biomolecular simulation
645 program. *J Comput Chem,* **30**:1545-1614. doi:10.1002/jcc.21287
646 Chakrabarti M, Jang H, Nussinov R. 2016. Comparison of the Conformations of KRAS
647 Isoforms, K-Ras4A and K-Ras4B, Points to Similarities and Significant Differences. *J*
648 *Phys Chem B,* **120**:667-679. doi:10.1021/acs.jpcb.5b11110
649 Chalhoub N, Baker SJ. 2009. PTEN and the PI3-kinase pathway in cancer. *Annu Rev Pathol,*
650 **4**:127-150. doi:10.1146/annurev.pathol.4.110807.092311
651 Chavan TS, Jang H, Khavrutskii L, Abraham SJ, Banerjee A, Freed BC, Johannessen L, Tarasov
652 SG, Gaponenko V, Nussinov R, Tarasova NI. 2015. High-Affinity Interaction of the K-
653 Ras4B Hypervariable Region with the Ras Active Site. *Biophys J,* **109**:2602-2613.
654 doi:10.1016/j.bpj.2015.09.034
655 Chen Z, Dempsey DR, Thomas SN, Hayward D, Bolduc DM, Cole PA. 2016. Molecular
656 Features of Phosphatase and Tensin Homolog (PTEN) Regulation by C-terminal
657 Phosphorylation. *J Biol Chem,* **291**:14160-14169. doi:10.1074/jbc.M116.728980
658 Chia JY, Gajewski JE, Xiao Y, Zhu HJ, Cheng HC. 2010. Unique biochemical properties of the
659 protein tyrosine phosphatase activity of PTEN-demonstration of different active site
660 structural requirements for phosphopeptide and phospholipid phosphatase activities of
661 PTEN. *Biochim Biophys Acta,* **1804**:1785-1795. doi:10.1016/j.bbapap.2010.05.009
662 Darden T, York D, Pedersen L. 1993. Particle Mesh Ewald - an N.Log(N) Method for Ewald
663 Sums in Large Systems. *J Chem Phys,* **98**:10089-10092. doi:Doi 10.1063/1.464397
664 Denning G, Jean-Joseph B, Prince C, Durden DL, Vogt PK. 2007. A short N-terminal sequence
665 of PTEN controls cytoplasmic localization and is required for suppression of cell growth.
666 *Oncogene,* **26**:3930-3940. doi:10.1038/sj.onc.1210175
667 Denu JM, Stuckey JA, Saper MA, Dixon JE. 1996. Form and function in protein
668 dephosphorylation. *Cell,* **87**:361-364. doi:10.1016/s0092-8674(00)81356-2
669 Dillon LM, Miller TW. 2014. Therapeutic targeting of cancers with loss of PTEN function. *Curr*
670 *Drug Targets,* **15**:65-79. doi:10.2174/1389450114666140106100909

671 Frishman D, Argos P. 1995. Knowledge-based protein secondary structure assignment. *Proteins,*
672 **23**:566-579. doi:10.1002/prot.340230412
673 Fruman DA, Chiu H, Hopkins BD, Bagrodia S, Cantley LC, Abraham RT. 2017. The PI3K
674 Pathway in Human Disease. *Cell,* **170**:605-635. doi:10.1016/j.cell.2017.07.029
675 Georgescu MM, Kirsch KH, Akagi T, Shishido T, Hanafusa H. 1999. The tumor-suppressor
676 activity of PTEN is regulated by its carboxyl-terminal region. *Proc Natl Acad Sci U S A,*
677 **96**:10182-10187. doi:10.1073/pnas.96.18.10182
678 Heinrich F, Chakravarthy S, Nanda H, Papa A, Pandolfi PP, Ross AH, Harishchandra RK,
679 Gericke A, Losche M. 2015. The PTEN Tumor Suppressor Forms Homodimers in
680 Solution. *Structure,* **23**:1952-1957.
681 Huang J, Rauscher S, Nawrocki G, Ran T, Feig M, de Groot BL, Grubmuller H, MacKerell AD,
682 Jr. 2017. CHARMM36m: an improved force field for folded and intrinsically disordered
683 proteins. *Nat Methods,* **14**:71-73. doi:10.1038/nmeth.4067
684 Huang J, Yan J, Zhang J, Zhu S, Wang Y, Shi T, Zhu C, Chen C, Liu X, Cheng J, Mustelin T,
685 Feng GS, Chen G, Yu J. 2012. SUMO1 modification of PTEN regulates tumorigenesis
686 by controlling its association with the plasma membrane. *Nat Commun,* **3**:911.
687 doi:10.1038/ncomms1919
688 Jang H, Abraham SJ, Chavan TS, Hitchinson B, Khavrutskii L, Tarasova NI, Nussinov R,
689 Gaponenko V. 2015. Mechanisms of membrane binding of small GTPase K-Ras4B
690 farnesylated hypervariable region. *J Biol Chem,* **290**:9465-9477.
691 doi:10.1074/jbc.M114.620724
692 Jang H, Banerjee A, Chavan T, Gaponenko V, Nussinov R. 2017. Flexible-body motions of
693 calmodulin and the farnesylated hypervariable region yield a high-affinity interaction
694 enabling K-Ras4B membrane extraction. *J Biol Chem,* **292**:12544-12559.
695 doi:10.1074/jbc.M117.785063
696 Jang H, Banerjee A, Chavan TS, Lu S, Zhang J, Gaponenko V, Nussinov R. 2016a. The higher
697 level of complexity of K-Ras4B activation at the membrane. *FASEB J,* **30**:1643-1655.
698 doi:10.1096/fj.15-279091
699 Jang H, Banerjee A, Marcus K, Makowski L, Mattos C, Gaponenko V, Nussinov R. 2019. The
700 Structural Basis of the Farnesylated and Methylated KRas4B Interaction with
701 Calmodulin. *Structure,* **27**:1647-1659. doi:10.1016/j.str.2019.08.009
702 Jang H, Muratcioglu S, Gursoy A, Keskin O, Nussinov R. 2016b. Membrane-associated Ras
703 dimers are isoform-specific: K-Ras dimers differ from H-Ras dimers. *Biochem J,*
704 **473**:1719-1732. doi:10.1042/BCJ20160031
705 Jang H, Zhang M, Nussinov R. 2020. The quaternary assembly of KRas4B with Raf-1 at the
706 membrane. *Comput Struct Biotechnol J,* **18**:737-748. doi:10.1016/j.csbj.2020.03.018
707 Kalli AC, Devaney I, Sansom MSP. 2014. Interactions of Phosphatase and Tensin Homologue
708 (PTEN) Proteins with Phosphatidylinositol Phosphates: Insights from Molecular
709 Dynamics Simulations of PTEN and Voltage Sensitive Phosphatase. *Biochemistry,*
710 **53**:1724-1732. doi:10.1021/bi5000299
711 Klauda JB, Venable RM, Freites JA, O'Connor JW, Tobias DJ, Mondragon-Ramirez C,
712 Vorobyov I, MacKerell AD, Jr., Pastor RW. 2010. Update of the CHARMM all-atom
713 additive force field for lipids: validation on six lipid types. *J Phys Chem B,* **114**:7830-
714 7843. doi:10.1021/jp101759q

715 Kotelevets L, Trifault B, Chastre E, Scott MGH. 2020. Posttranslational Regulation and
716 Conformational Plasticity of PTEN. *Cold Spring Harb Perspect Med,* **10**.
717 doi:10.1101/cshperspect.a036095
718 Lee CU, Hahne G, Hanske J, Bange T, Bier D, Rademacher C, Hennig S, Grossmann TN. 2015.
719 Redox Modulation of PTEN Phosphatase Activity by Hydrogen Peroxide and
720 Bisperoxidovanadium Complexes. *Angewandte Chemie-International Edition,* **54**:13796-
721 13800. doi:10.1002/anie.201506338
722 Lee JO, Yang H, Georgescu MM, Di Cristofano A, Maehama T, Shi Y, Dixon JE, Pandolfi P,
723 Pavletich NP. 1999. Crystal structure of the PTEN tumor suppressor: implications for its
724 phosphoinositide phosphatase activity and membrane association. *Cell,* **99**:323-334.
725 doi:10.1016/s0092-8674(00)81663-3
726 Liao TJ, Jang H, Fushman D, Nussinov R. 2018. Allosteric KRas4B Can Modulate SOS1 Fast
727 and Slow Ras Activation Cycles. *Biophys J,* **115**:629-641. doi:10.1016/j.bpj.2018.07.016
728 Liao TJ, Jang H, Tsai CJ, Fushman D, Nussinov R. 2017. The dynamic mechanism of RASSF5
729 and MST kinase activation by Ras. *Phys Chem Chem Phys,* **19**:6470-6480.
730 doi:10.1039/c6cp08596b
731 Liu J, Nussinov R. 2008. Allosteric effects in the marginally stable von Hippel-Lindau tumor
732 suppressor protein and allostery-based rescue mutant design. *Proc Natl Acad Sci U S A,*
733 **105**:901-906. doi:10.1073/pnas.0707401105
734 Lu S, Banerjee A, Jang H, Zhang J, Gaponenko V, Nussinov R. 2015. GTP Binding and
735 Oncogenic Mutations May Attenuate Hypervariable Region (HVR)-Catalytic Domain
736 Interactions in Small GTPase K-Ras4B, Exposing the Effector Binding Site. *J Biol Chem,*
737 **290**:28887-28900. doi:10.1074/jbc.M115.664755
738 Lu S, Jang H, Nussinov R, Zhang J. 2016. The Structural Basis of Oncogenic Mutations G12,
739 G13 and Q61 in Small GTPase K-Ras4B. *Sci Rep,* **6**:21949. doi:10.1038/srep21949
740 Lumb CN, Sansom MSP. 2013. Defining the Membrane-Associated State of the PTEN Tumor
741 Suppressor Protein. *Biophysical Journal,* **104**:613-621.
742 Malaney P, Pathak RR, Xue B, Uversky VN, Dave V. 2013. Intrinsic disorder in PTEN and its
743 interactome confers structural plasticity and functional versatility. *Sci Rep,* **3**:2035.
744 doi:10.1038/srep02035
745 Masson GR, Perisic O, Burke JE, Williams RL. 2016. The intrinsically disordered tails of PTEN
746 and PTEN-L have distinct roles in regulating substrate specificity and membrane activity.
747 *Biochem J,* **473**:135-144. doi:10.1042/BJ20150931
748 Masson GR, Williams RL. 2020. Structural Mechanisms of PTEN Regulation. *Cold Spring Harb*
749 *Perspect Med,* **10**. doi:10.1101/cshperspect.a036152
750 McLoughlin NM, Mueller C, Grossmann TN. 2018. The Therapeutic Potential of PTEN
751 Modulation: Targeting Strategies from Gene to Protein. *Cell Chemical Biology,* **25**:19-29.
752 doi:10.1016/j.chembiol.2017.10.009
753 Mingo J, Luna S, Gaafar A, Nunes-Xavier CE, Torices L, Mosteiro L, Ruiz R, Guerra I, Llarena
754 R, Angulo JC, Lopez JI, Pulido R. 2019. Precise definition of PTEN C-terminal epitopes
755 and its implications in clinical oncology. *NPJ Precis Oncol,* **3**:11. doi:10.1038/s41698-
756 019-0083-4
757 Muratcioglu S, Jang H, Gursoy A, Keskin O, Nussinov R. 2017. PDEdelta Binding to Ras
758 Isoforms Provides a Route to Proper Membrane Localization. *J Phys Chem B,* **121**:5917-
759 5927. doi:10.1021/acs.jpcb.7b03035

760 Myers MP, Pass I, Batty IH, Van der Kaay J, Stolarov JP, Hemmings BA, Wigler MH, Downes
761 CP, Tonks NK. 1998. The lipid phosphatase activity of PTEN is critical for its tumor
762 supressor function. *Proc Natl Acad Sci U S A,* **95**:13513-13518.
763 doi:10.1073/pnas.95.23.13513
764 Nguyen HN, Afkari Y, Senoo H, Sesaki H, Devreotes PN, Iijima M. 2014a. Mechanism of
765 human PTEN localization revealed by heterologous expression in Dictyostelium.
766 *Oncogene,* **33**:5688-5696. doi:10.1038/onc.2013.507
767 Nguyen HN, Yang JM, Afkari Y, Park BH, Sesaki H, Devreotes PN, Iijima M. 2014b.
768 Engineering ePTEN, an enhanced PTEN with increased tumor suppressor activities. *Proc*
769 *Natl Acad Sci U S A,* **111**:E2684-2693. doi:10.1073/pnas.1409433111
770 Nguyen HN, Yang JM, Jr., Rahdar M, Keniry M, Swaney KF, Parsons R, Park BH, Sesaki H,
771 Devreotes PN, Iijima M. 2015. A new class of cancer-associated PTEN mutations
772 defined by membrane translocation defects. *Oncogene,* **34**:3737-3743.
773 doi:10.1038/onc.2014.293
774 Nussinov R, Zhang M, Tsai C-J, Jang H. 2020. Phosphorylation and Driver Mutations in PI3Kα
775 and PTEN Autoinhibition. *Mol Cancer Res*. doi:10.1158/1541-7786.MCR-20-0818
776 Okumura K, Mendoza M, Bachoo RM, DePinho RA, Cavenee WK, Furnari FB. 2006. PCAF
777 modulates PTEN activity. *J Biol Chem,* **281**:26562-26568. doi:10.1074/jbc.M605391200
778 Ozdemir ES, Jang H, Gursoy A, Keskin O, Li Z, Sacks DB, Nussinov R. 2018a. Unraveling the
779 molecular mechanism of interactions of the Rho GTPases Cdc42 and Rac1 with the
780 scaffolding protein IQGAP2. *J Biol Chem,* **293**:3685-3699.
781 doi:10.1074/jbc.RA117.001596
782 Ozdemir ES, Jang H, Gursoy A, Keskin O, Nussinov R. 2018b. Arl2-Mediated Allosteric
783 Release of Farnesylated KRas4B from Shuttling Factor PDEdelta. *J Phys Chem B,*
784 **122**:7503-7513. doi:10.1021/acs.jpcb.8b04347
785 Phillips JC, Braun R, Wang W, Gumbart J, Tajkhorshid E, Villa E, Chipot C, Skeel RD, Kale L,
786 Schulten K. 2005. Scalable molecular dynamics with NAMD. *J Comput Chem,* **26**:1781-
787 1802. doi:10.1002/jcc.20289
788 Rahdar M, Inoue T, Meyer T, Zhang J, Vazquez F, Devreotes PN. 2009. A phosphorylation-
789 dependent intramolecular interaction regulates the membrane association and activity of
790 the tumor suppressor PTEN. *Proc Natl Acad Sci U S A,* **106**:480-485.
791 doi:10.1073/pnas.0811212106
792 Rodriguez-Escudero I, Oliver MD, Andres-Pons A, Molina M, Cid VJ, Pulido R. 2011. A
793 comprehensive functional analysis of PTEN mutations: implications in tumor- and
794 autism-related syndromes. *Hum Mol Genet,* **20**:4132-4142. doi:10.1093/hmg/ddr337
795 Ross AH, Gericke A. 2009. Phosphorylation keeps PTEN phosphatase closed for business. *Proc*
796 *Natl Acad Sci U S A,* **106**:1297-1298. doi:10.1073/pnas.0812473106
797 Roy A, Kucukural A, Zhang Y. 2010. I-TASSER: a unified platform for automated protein
798 structure and function prediction. *Nat Protoc,* **5**:725-738. doi:10.1038/nprot.2010.5
799 Ryckaert J-P, Ciccotti G, Berendsen HJC. 1977. Numerical integration of the cartesian equations
800 of motion of a system with constraints: molecular dynamics of n-alkanes. *J Comput Phys,*
801 **23**:327-341.
802 Shenoy SS, Nanda H, Losche M. 2012. Membrane association of the PTEN tumor suppressor:
803 Electrostatic interaction with phosphatidylserine-containing bilayers and regulatory role
804 of the C-terminal tail. *Journal of Structural Biology,* **180**:394-408.
805 doi:10.1016/j.jsb.2012.10.003

806 Smart OS, Goodfellow JM, Wallace BA. 1993. The pore dimensions of gramicidin A. *Biophys J,*
807 **65**:2455-2460. doi:10.1016/S0006-3495(93)81293-1
808 Smith IN, Thacker S, Jaini R, Eng C. 2019. Dynamics and structural stability effects of germline
809 PTEN mutations associated with cancer versus autism phenotypes. *J Biomol Struct Dyn,*
810 **37**:1766-1782. doi:10.1080/07391102.2018.1465854
811 Song MS, Salmena L, Pandolfi PP. 2012. The functions and regulation of the PTEN tumour
812 suppressor. *Nat Rev Mol Cell Biol,* **13**:283-296. doi:10.1038/nrm3330
813 Sun Z, Huang C, He J, Lamb KL, Kang X, Gu T, Shen WH, Yin Y. 2014. PTEN C-terminal
814 deletion causes genomic instability and tumor development. *Cell Rep,* **6**:844-854.
815 doi:10.1016/j.celrep.2014.01.030
816 Vazquez F, Ramaswamy S, Nakamura N, Sellers WR. 2000. Phosphorylation of the PTEN tail
817 regulates protein stability and function. *Mol Cell Biol,* **20**:5010-5018.
818 doi:10.1128/mcb.20.14.5010-5018.2000
819 Walker SM, Leslie NR, Perera NM, Batty IH, Downes CP. 2004. The tumour-suppressor
820 function of PTEN requires an N-terminal lipid-binding motif. *Biochem J,* **379**:301-307.
821 doi:10.1042/BJ20031839
822 Woolf TB, Roux B. 1994. Molecular dynamics simulation of the gramicidin channel in a
823 phospholipid bilayer. *Proc Natl Acad Sci U S A,* **91**:11631-11635.
824 doi:10.1073/pnas.91.24.11631
825 Woolf TB, Roux B. 1996. Structure, energetics, and dynamics of lipid-protein interactions: A
826 molecular dynamics study of the gramicidin A channel in a DMPC bilayer. *Proteins,*
827 **24**:92-114. doi:10.1002/(SICI)1097-0134(199601)24:1<92::AID-PROT7>3.0.CO;2-Q
828 Wu XW, Brooks BR. 2003. Self-guided Langevin dynamics simulation method. *Chem Phys Lett,*
829 **381**:512-518. doi:10.1016/j.cplett.2003.10.013
830 Xiao Y, Yeong Chit Chia J, Gajewski JE, Sio Seng Lio D, Mulhern TD, Zhu HJ, Nandurkar H,
831 Cheng HC. 2007. PTEN catalysis of phospholipid dephosphorylation reaction follows a
832 two-step mechanism in which the conserved aspartate-92 does not function as the general
833 acid--mechanistic analysis of a familial Cowden disease-associated PTEN mutation. *Cell*
834 *Signal,* **19**:1434-1445. doi:10.1016/j.cellsig.2007.01.021
835 Yang J, Yan R, Roy A, Xu D, Poisson J, Zhang Y. 2015. The I-TASSER Suite: protein structure
836 and function prediction. *Nat Methods,* **12**:7-8. doi:10.1038/nmeth.3213
837 Yang J, Zhang Y. 2015. I-TASSER server: new development for protein structure and function
838 predictions. *Nucleic Acids Res,* **43**:W174-181. doi:10.1093/nar/gkv342
839 Yehia L, Ngeow J, Eng C. 2019. PTEN-opathies: from biological insights to evidence-based
840 precision medicine. *J Clin Invest,* **129**:452-464. doi:10.1172/JCI121277
841 Yehia L, Ni Y, Sesock K, Niazi F, Fletcher B, Chen HJL, LaFramboise T, Eng C. 2018.
842 Unexpected cancer-predisposition gene variants in Cowden syndrome and Bannayan-
843 Riley-Ruvalcaba syndrome patients without underlying germline PTEN mutations. *PLoS*
844 *Genet,* **14**:e1007352. doi:10.1371/journal.pgen.1007352
845 Zhang M, Jang H, Gaponenko V, Nussinov R. 2017. Phosphorylated Calmodulin Promotes PI3K
846 Activation by Binding to the SH2 Domains. *Biophys J,* **113**:1956-1967.
847 doi:10.1016/j.bpj.2017.09.008
848 Zhang M, Jang H, Nussinov R. 2019a. The mechanism of PI3Kalpha activation at the atomic
849 level. *Chem Sci,* **10**:3671-3680. doi:10.1039/c8sc04498h
850 Zhang M, Jang H, Nussinov R. 2019b. The structural basis for Ras activation of PI3Kalpha lipid
851 kinase. *Phys Chem Chem Phys,* **21**:12021-12028. doi:10.1039/c9cp00101h

852 Zhang M, Jang H, Nussinov R. 2020. PI3K inhibitors: review and new strategies. *Chem Sci,*
853 **11**:5855-5865. doi:10.1039/d0sc01676d

854

855

856 **Figure 1.** PTEN sequence and structure.

857

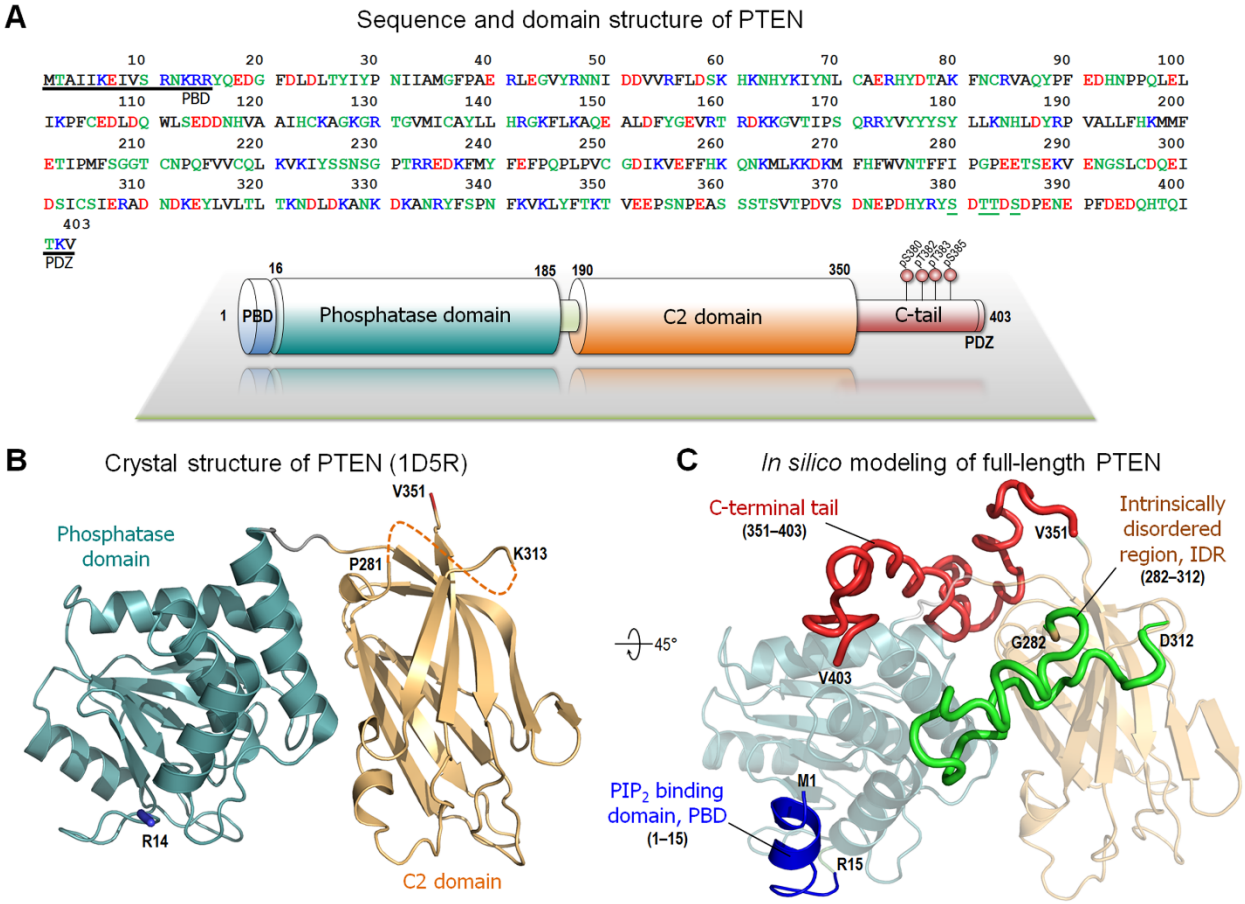


858

859

**Figure 2.** Membrane interaction of PTEN.

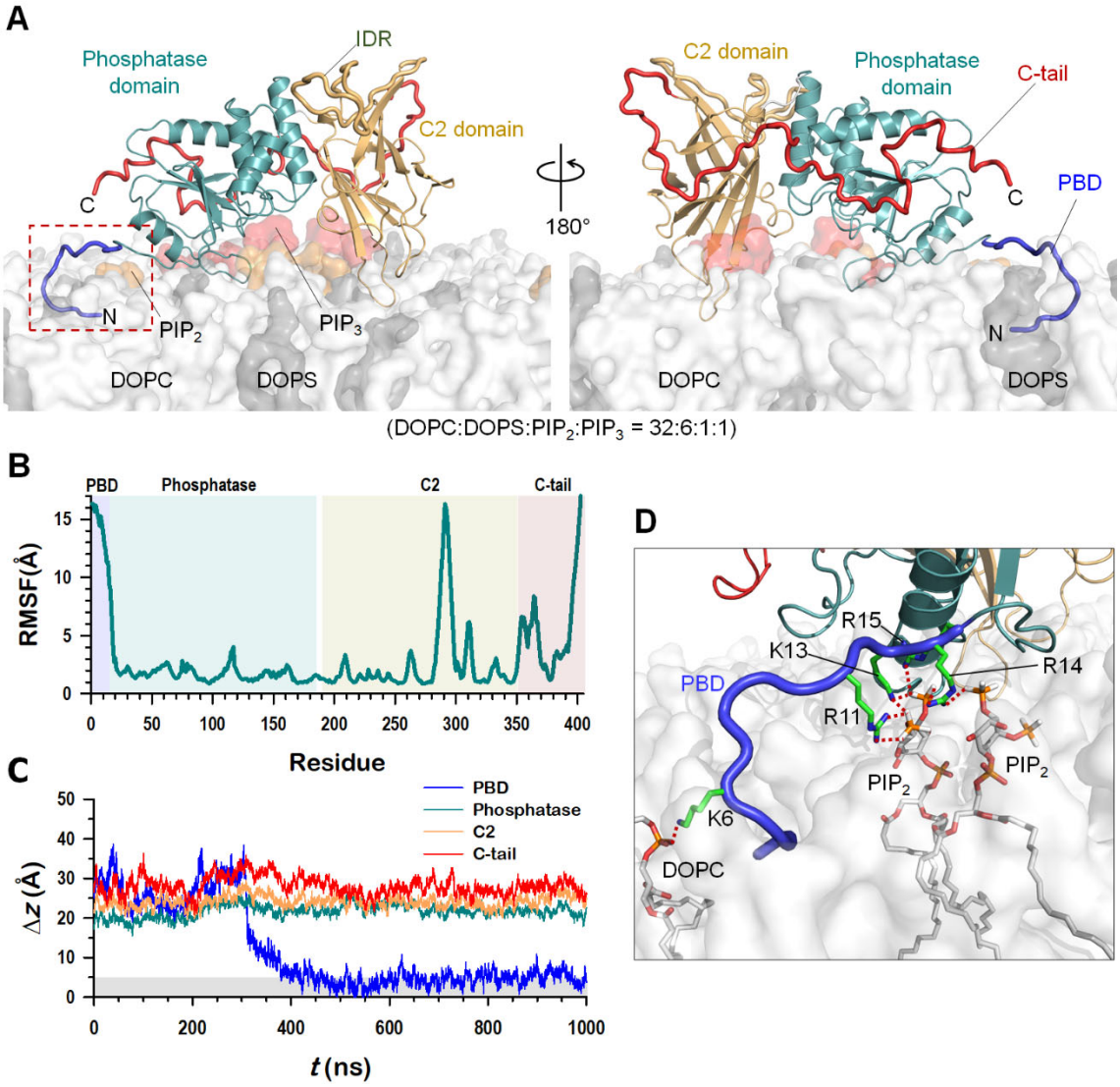

863 **Figure 3.** Lipid contact probability.

864

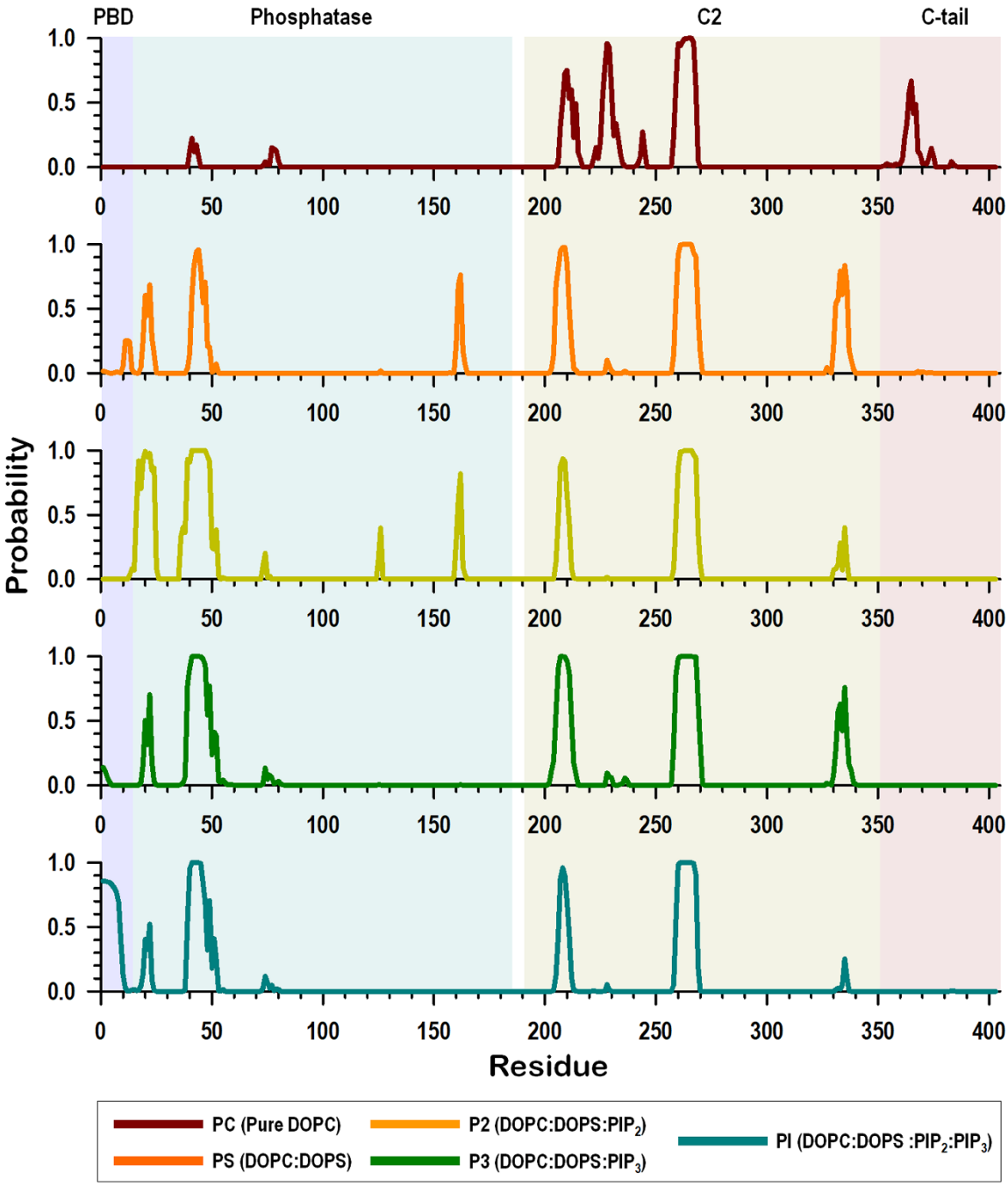


865

866

867 **Figure 4.** Salt bridge interactions of PTEN.

868

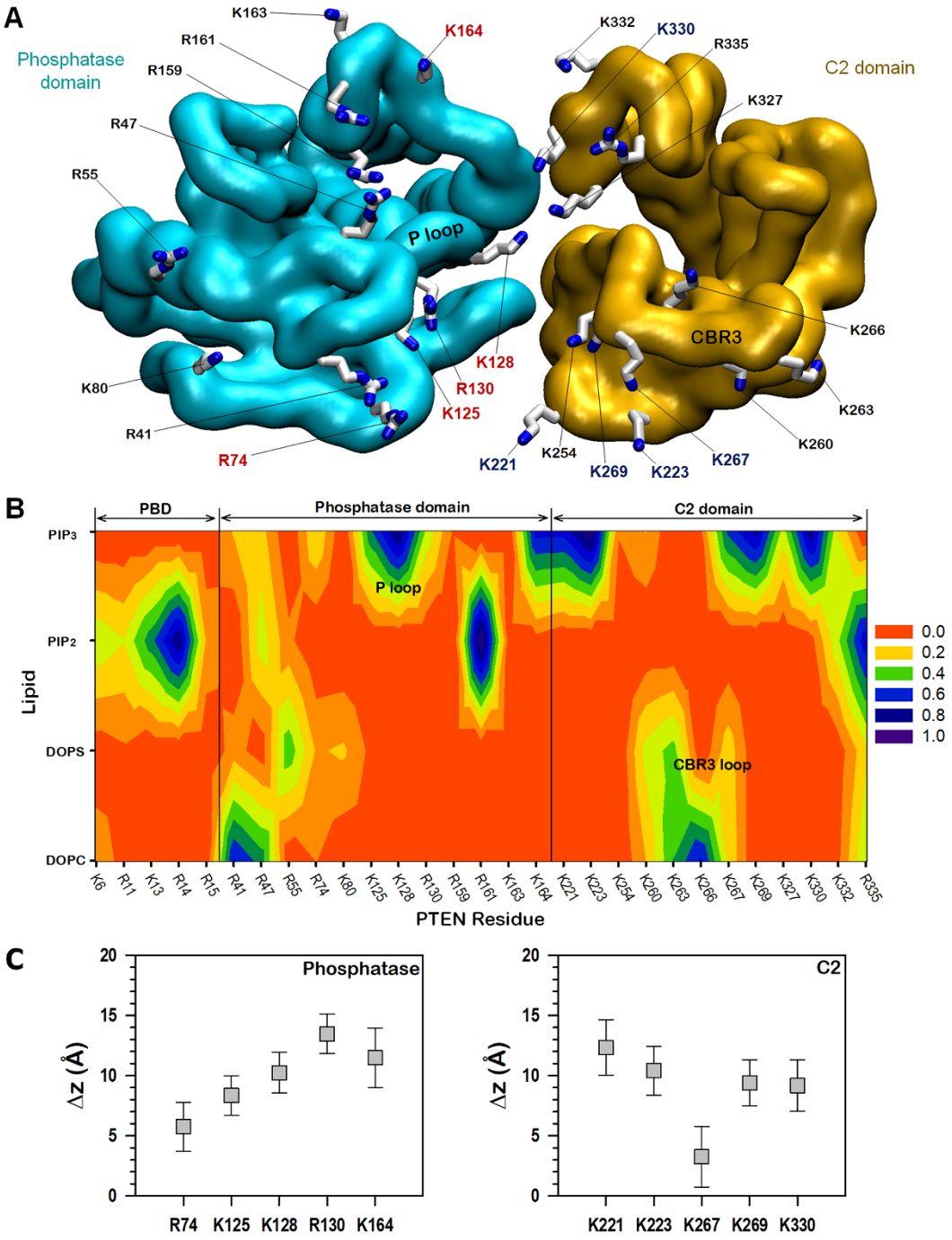


869

870 **Figure 5.** $PIP_3$ coordination induces the P loop conformational change.

871

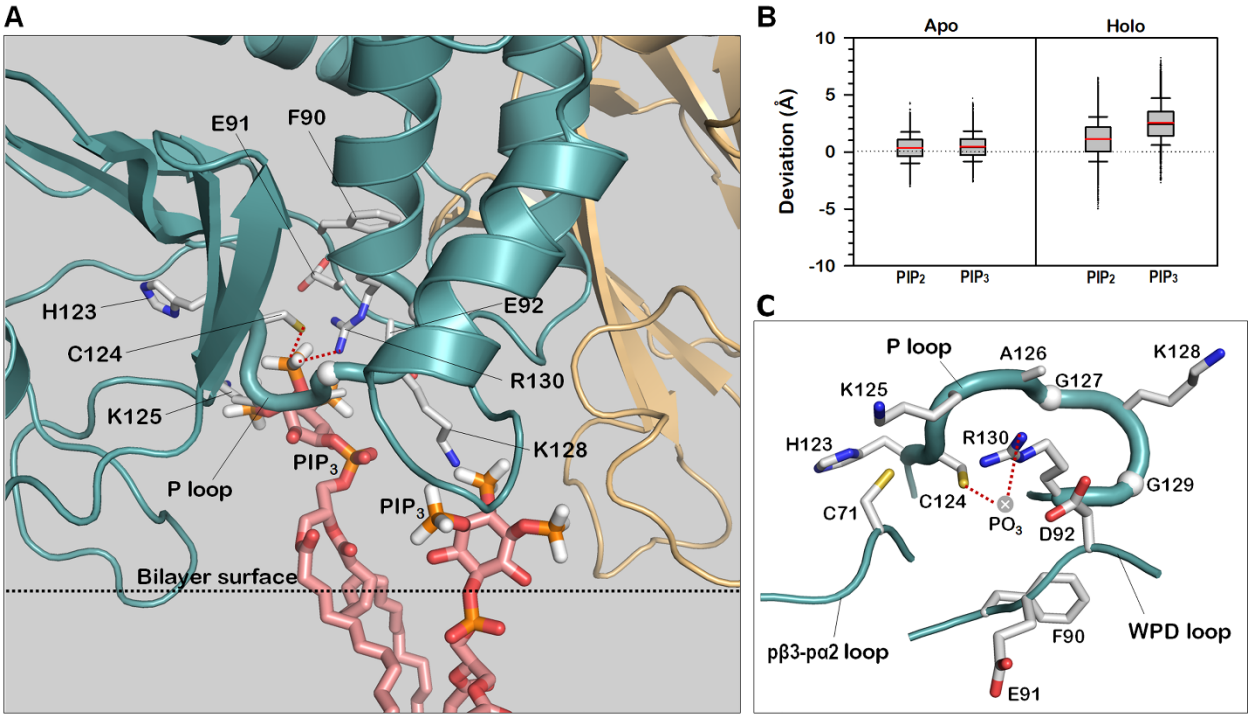


872

873

874 **Figure 6.** High density of waters at the active site for catalysis.

875

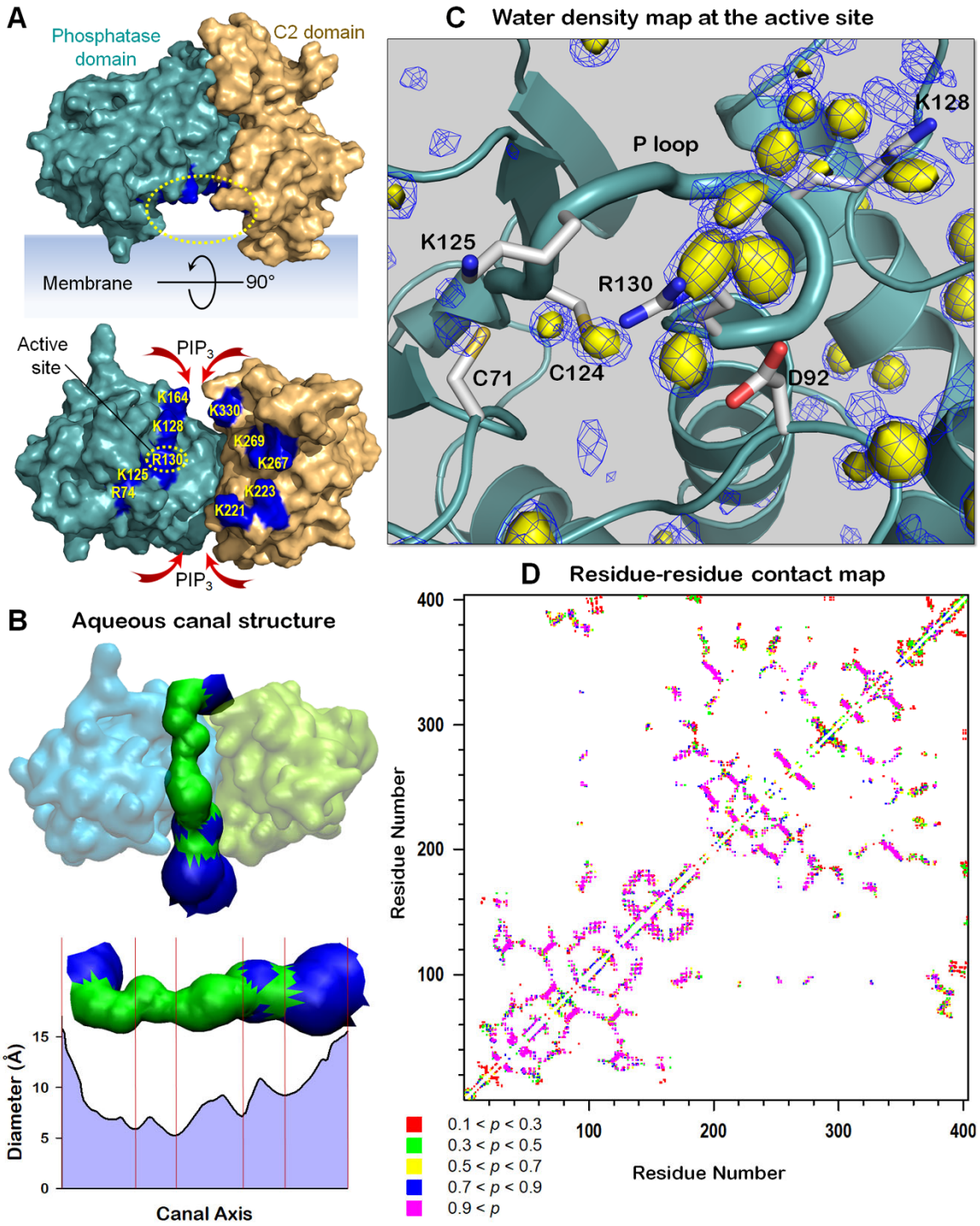


876

877

878 **Figure 7.** A schematic diagram illustrating membrane localization of PTEN.

879

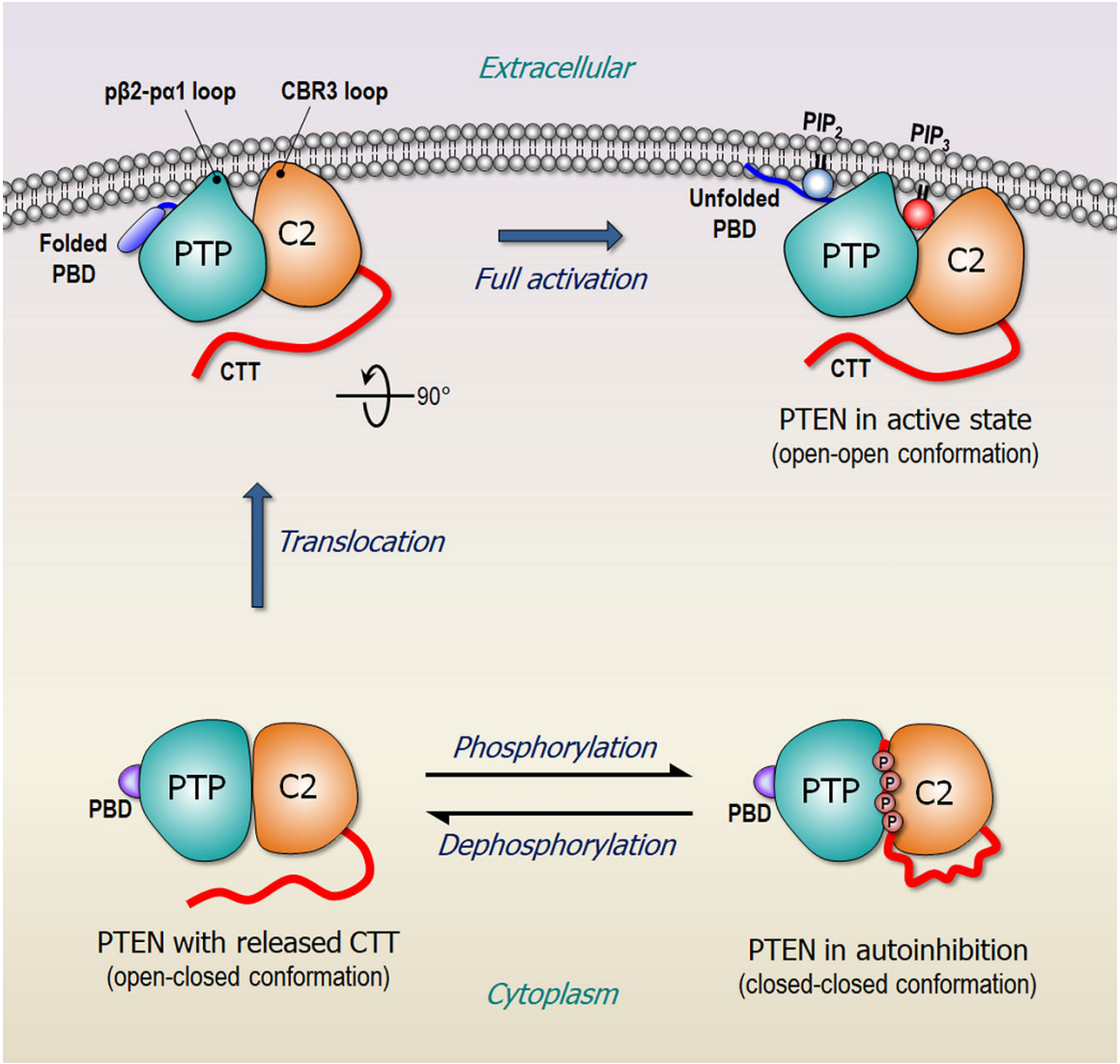


880

881

882 **Figure 2–figure supplement 1.** Initial configuration of the PTEN-membrane system.

883

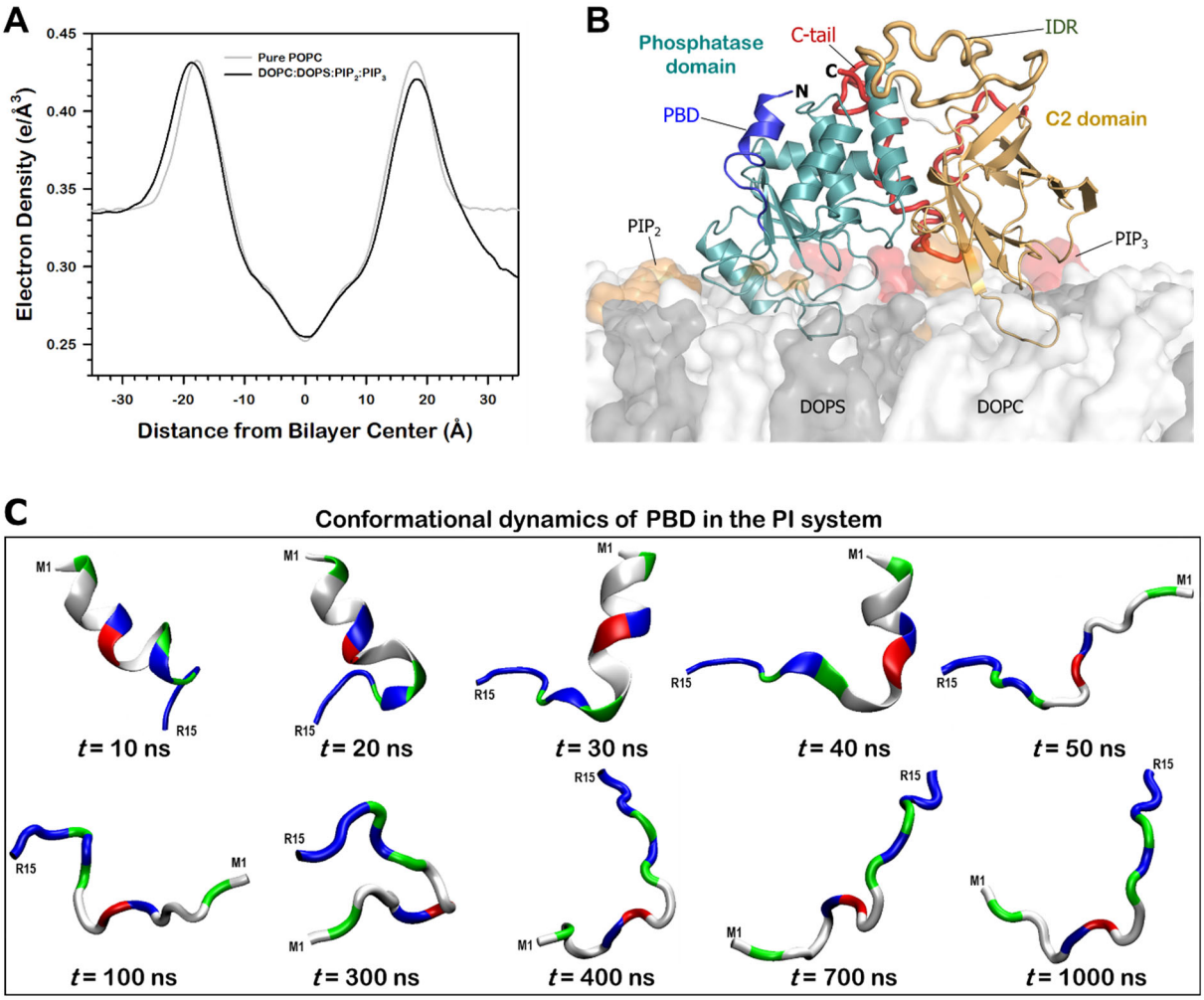


884

885

886 **Figure 3–figure supplement 2.** Relaxed PTEN conformations in different lipid bilayer systems.

887

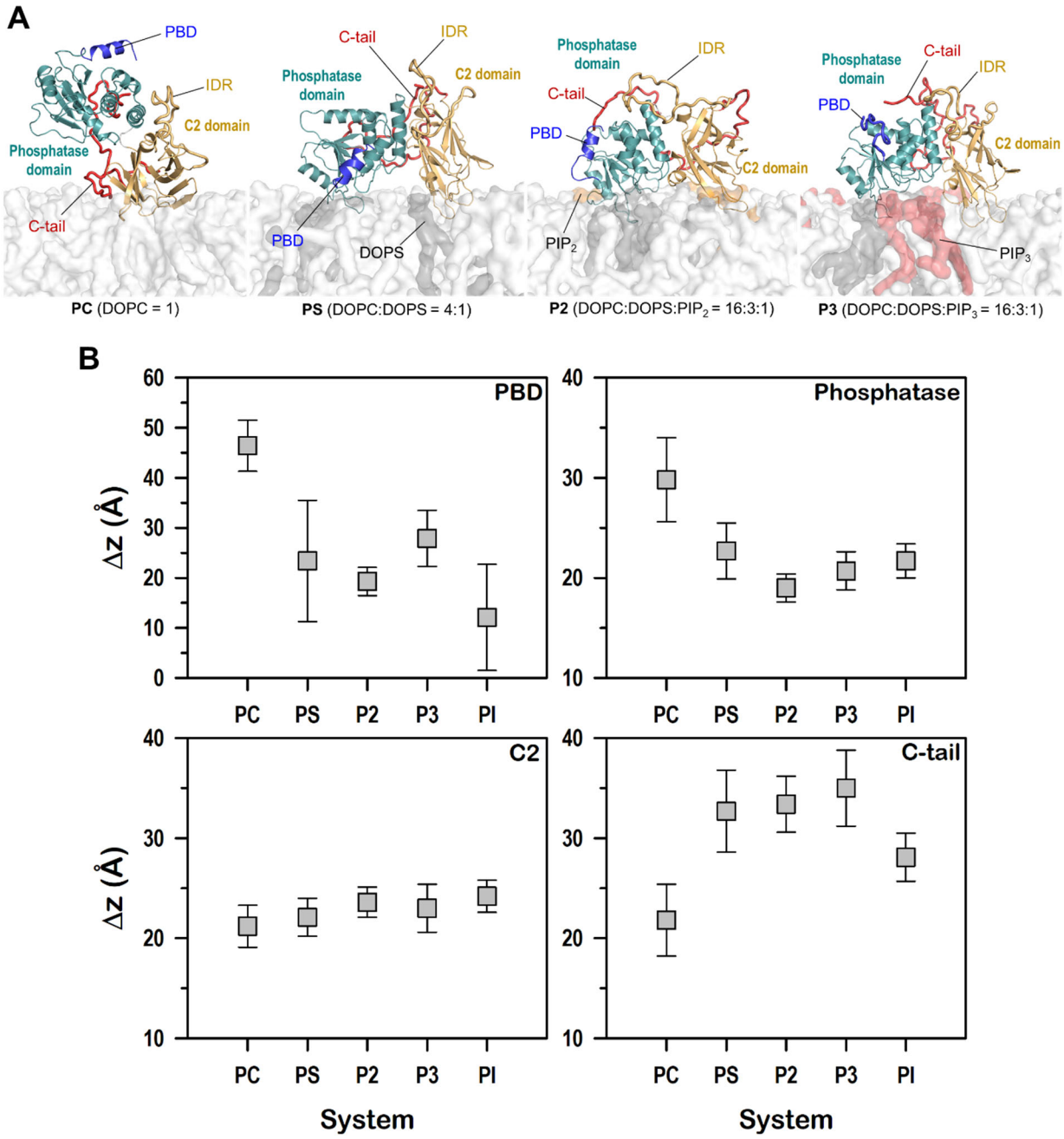


888

889

890 **Figure 3–figure supplement 3.** Helix tilt angle of PTEN.

891

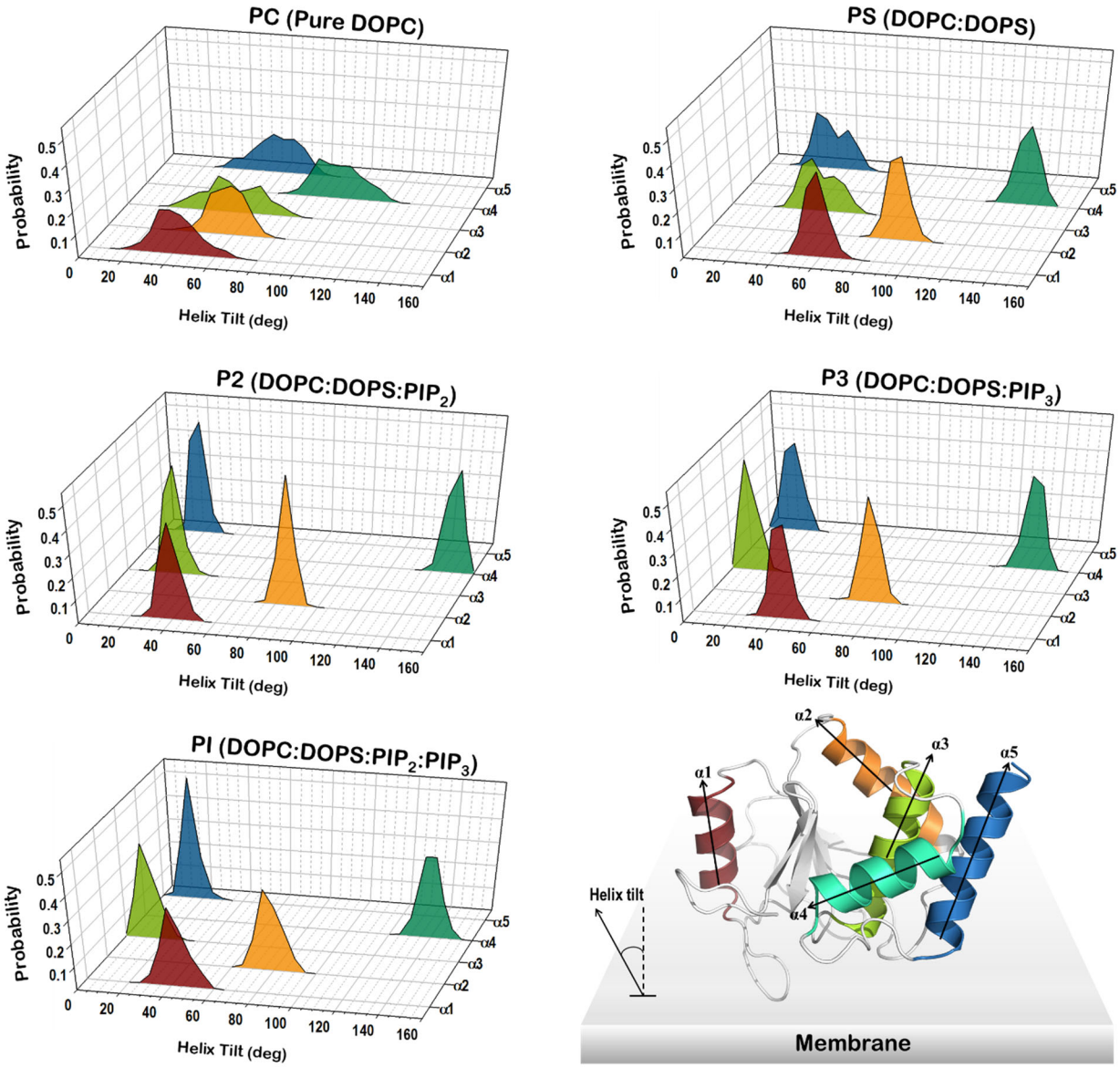


892

893

894 **Figure 3–figure supplement 4.** Conformational dynamics of PBD in different bilayer systems.

895

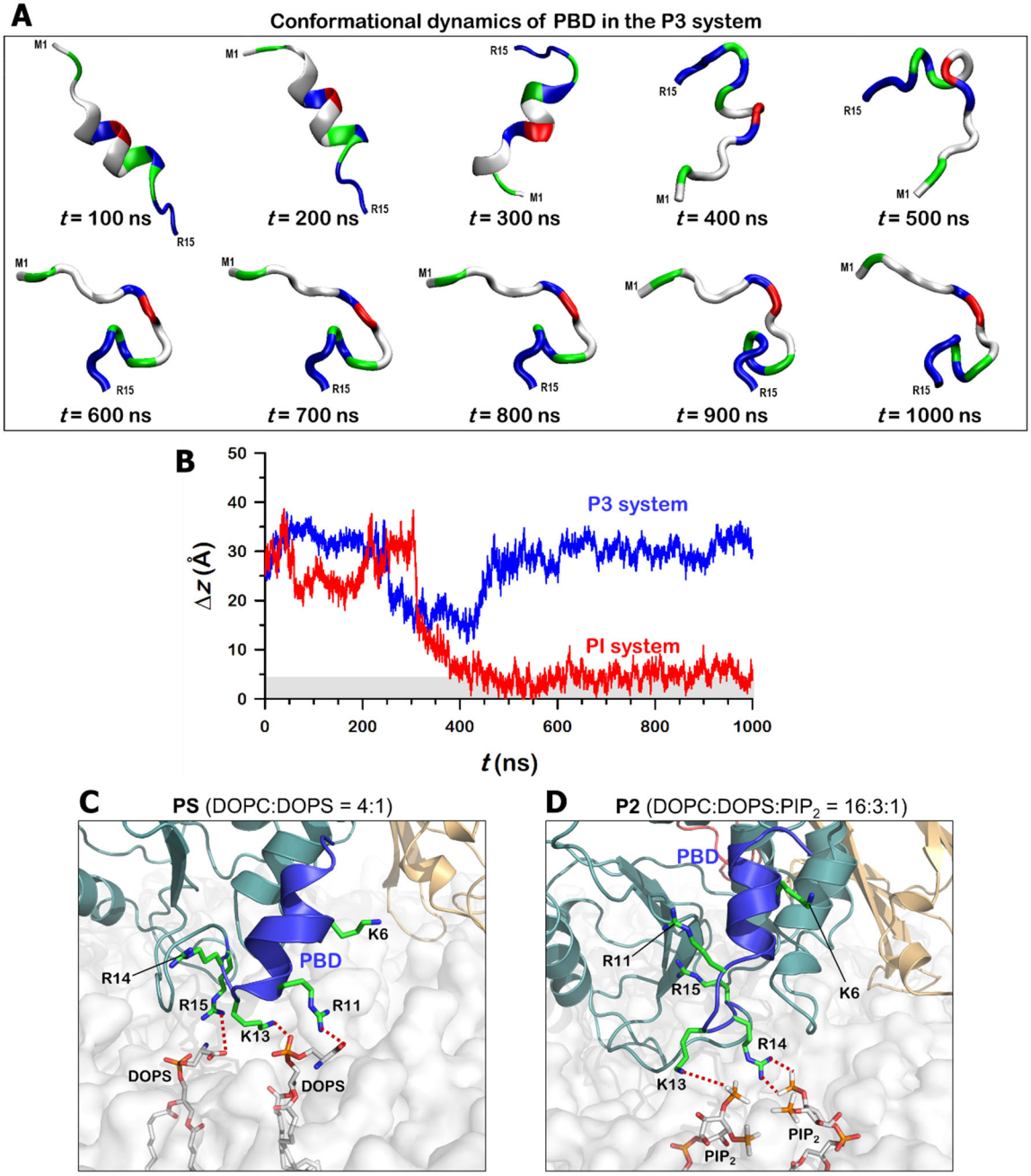


896

897

898 **Figure 4–figure supplement 5.** Salt bridge interactions of key basic residues.

899

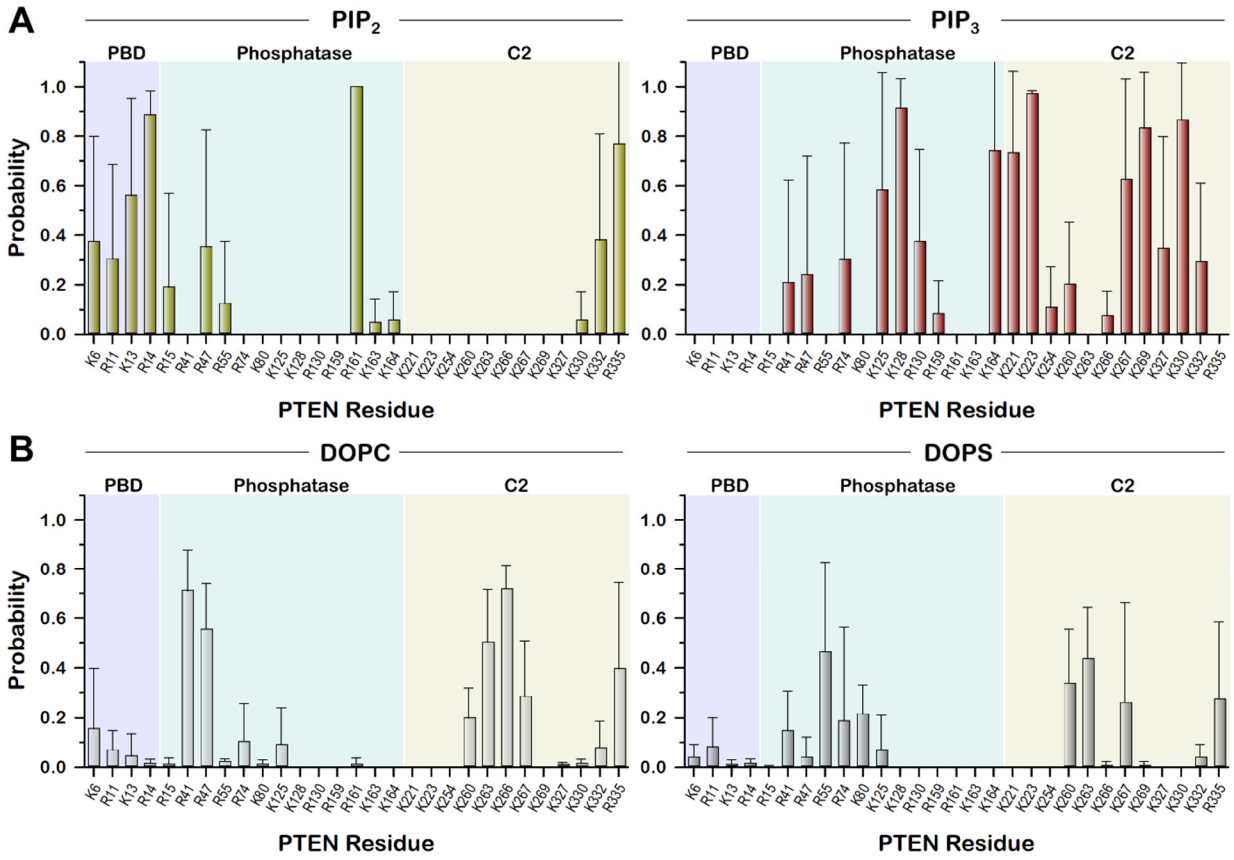


900

901

902 **Figure 5–figure supplement 6.** Conformational change of P loop in different bilayer systems.

903

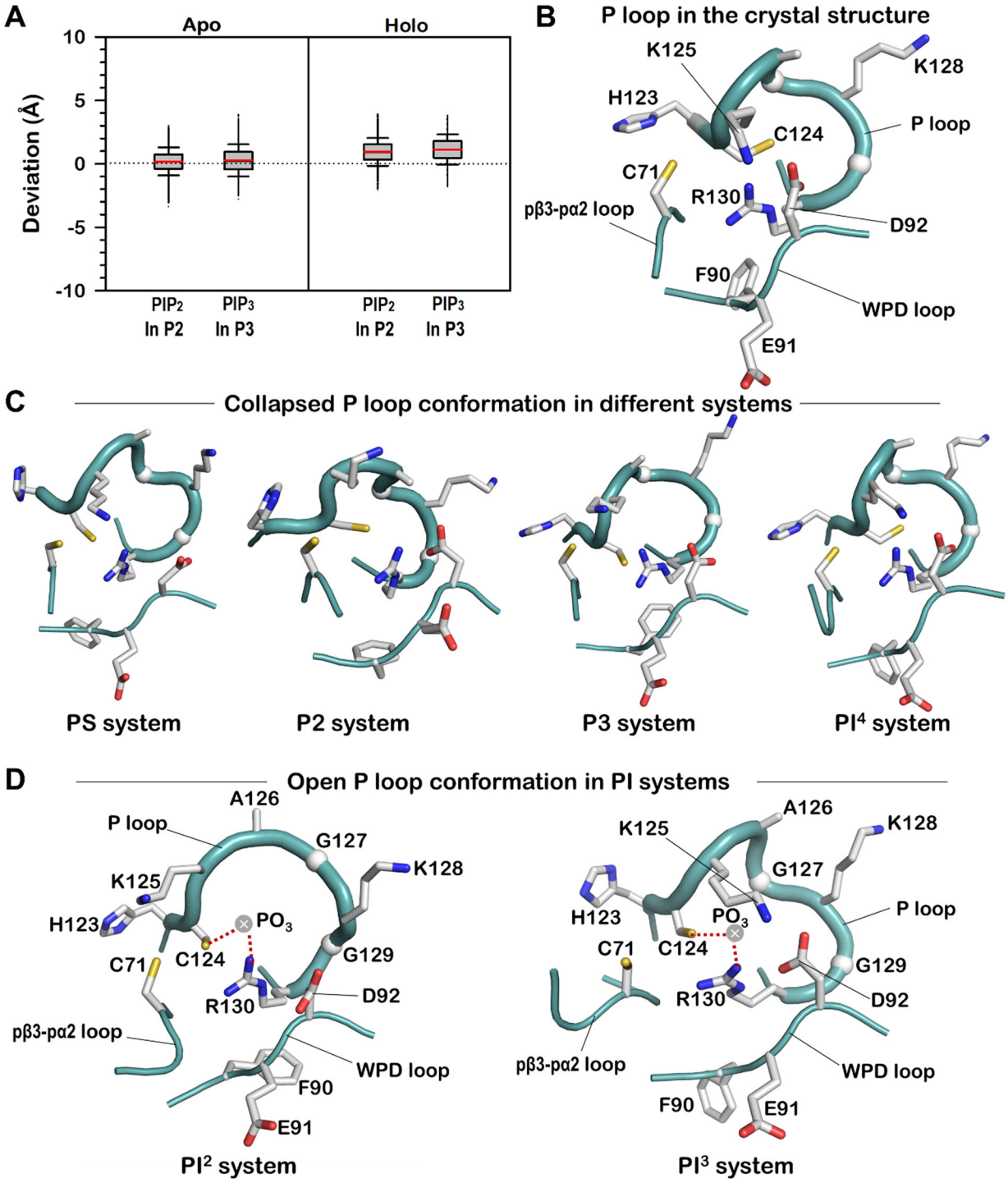


904

905

906 **Figure 6–figure supplement 7.** Density of waters at the active site in different bilayer systems.

907

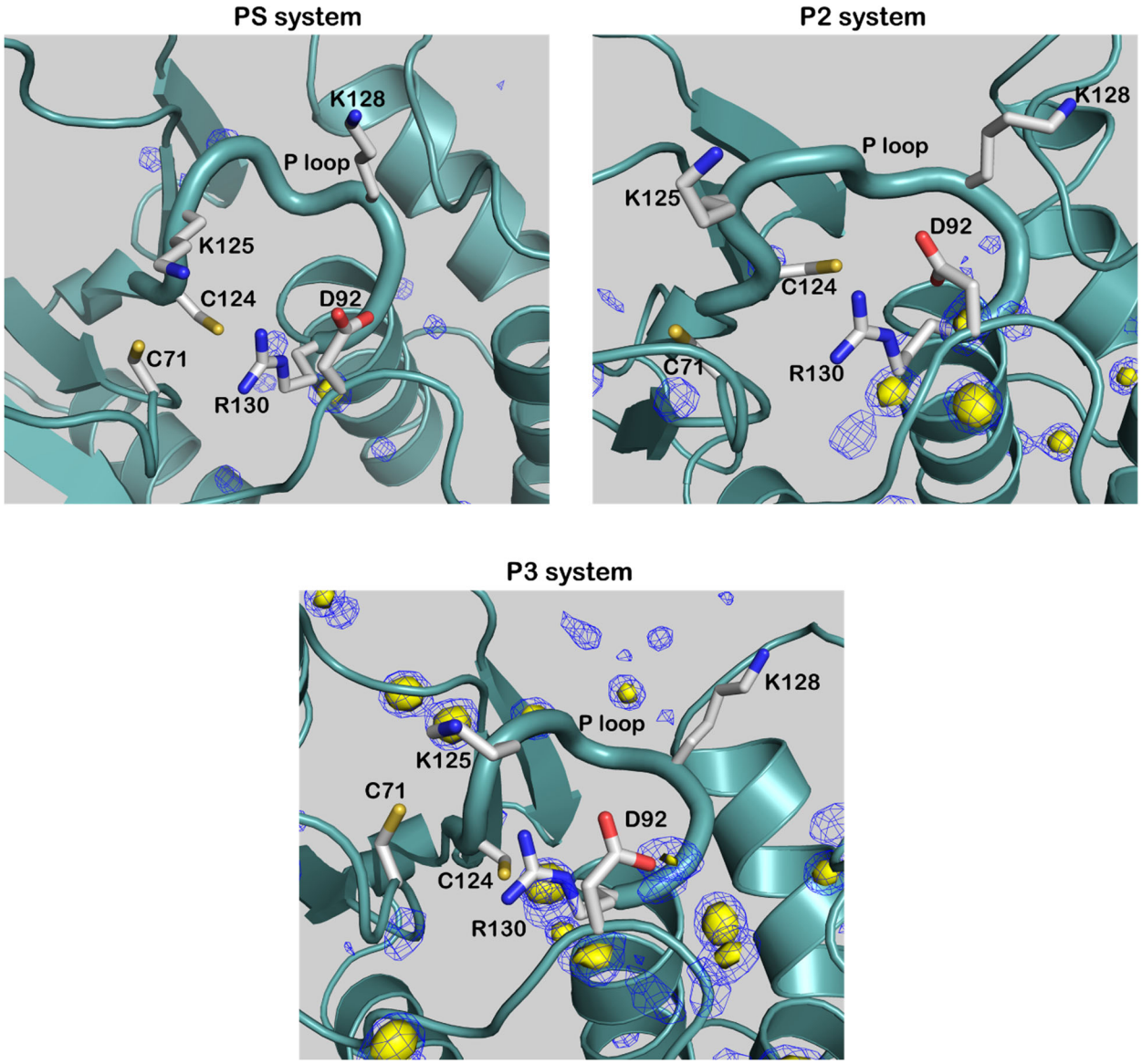


908

909

910 **Figure 6–figure supplement 8.** Conformations of IDR and CTT.

911

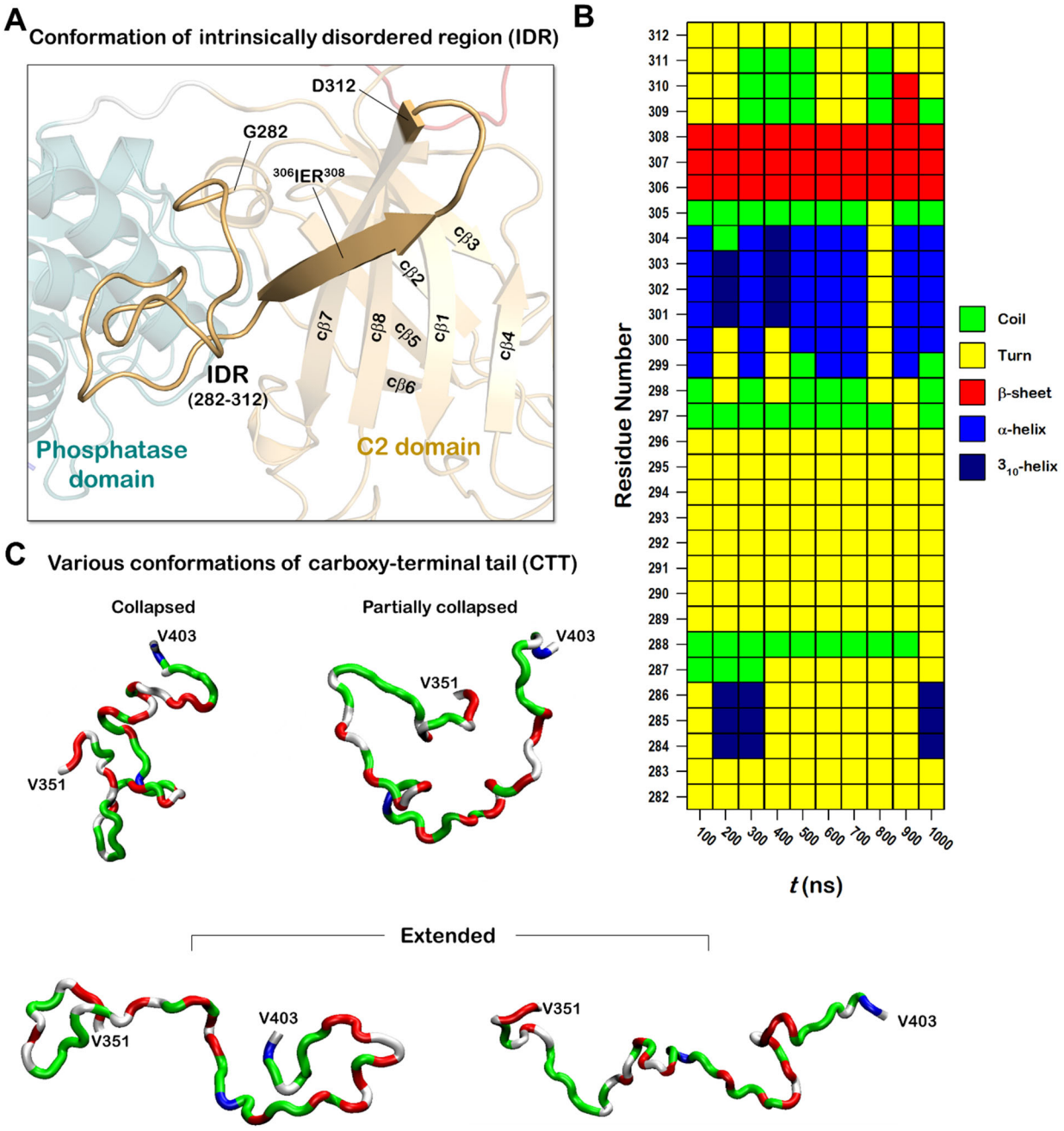


912